Bioorg. Med. Chem. 133 (2026) 118499

Contents lists available at ScienceDirect

Bioorganic & Medicinal Chemistry

journal homepage: www.elsevier.com/locate/bmc

Discovery of novel hybrids of coumarin and quinoline as potential anti-Alzheimer's disease agent

Shun Li [1], Xinrui Li [1], Shuanglong Li, Daoyuan Chen [*], Chunli Xia [*]

School of Bioengineering, Zhuhai Campus of Zunyi medical University, Zhuhai 519041, China

ARTICLE INFO

Keywords:
Alzheimer's disease
Multi-target-directed ligands
Coumarin-quinoline hybrid
Amyloid-β protein
β-secretase 1

ABSTRACT

The multifaceted nature of Alzheimer's disease (AD) spurred growing interest in developing multi-target-directed ligands (MTDLs) for its prevention and treatment. Coumarin and quinoline scaffolds, recognized for their broad spectrum of AD-related biological activities including amyloid-β (Aβ) aggregation regulation, cholinesterase (ChE) inhibition, β-secretase 1 (BACE1) inhibition and neuroprotection, were identified as potential building blocks. Here in this study, 24 novel coumarin-quinoline hybrid compounds were rationally designed and synthesized. Inhibition studies targeting Aβ, ChE and BACE1 identified compound **B8** as a promising lead compound. **B8** exhibited effective binding to Aβ, and significantly attenuated Aβ-induced SH-SY5Y cell death by lowering oxidative stress and decreasing cellular apoptosis. Crucially, **B8** demonstrated excellent blood-brain barrier (BBB) permeability, and intragastric administration of **B8** to 7-month-old APP/PS1 transgenic mice resulted in improved cognitive function. This improvement was supported by the protection of hippocampal and cortical neurons from necrosis, attenuation of oxidative stress and inflammation in these brain regions, as well as a reduction in Aβ deposition. These findings highlight the potential of coumarin-quinoline hybrids as a novel class of AD therapeutics, with **B8** emerging as a promising lead candidate warranting further investigation.

1. Introduction

Alzheimer's disease (AD), characterized by progressive neurodegeneration, stands as the predominant cause of dementia among the elderly population. Pathological mechanisms of AD involve several key factors: abnormal accumulation of amyloid-beta (Aβ), disturbances in cholinergic neurotransmission, oxidative stress, and neuroinflammation.[1–4] Crucially, these factors are interconnected within a self-perpetuating neurotoxic cascade. For example, β-site amyloid precursor protein-cleaving enzyme 1 (BACE1)-mediated amyloid precursor protein (APP) cleavage increases the formation of soluble Aβ oligomers and fibrils, thereby promoting Aβ deposition and exacerbating neurotoxicity linked to oxidative stress. Excess reactive oxygen species (ROS), in turn upregulate BACE1 activity and accelerate abnormal tau phosphorylation and aggregation. Concurrently, hyperactive cholinesterases (ChEs) reduce synaptic acetylcholine (ACh) level, weakening cholinergic anti-inflammatory and neuroprotective regulation while also promoting Aβ aggregation, thus forming a vicious cycle.[5–8]Conventional pharmacological interventions focusing on singular pathological aspects, such as acetylcholinesterase inhibitors or *N*-methyl-D-aspartate (NMDA) receptor antagonists, have exhibited constrained clinical effectiveness, attributed to multifactorial etiology of the disease.[9] This has spurred an growing interest in the development of multi-target-directed ligands (MTDLs) as a more holistic therapeutic strategy.[10,11]

The persistent lack of effective therapeutic interventions for AD has driven extensive investigation into various natural and synthetic scaffolds.[12] Among these, coumarin and quinoline have emerged as promising scaffold for AD drug discovery. Derivatives of both scaffolds display a broad spectrum of AD-related biological activities, including inhibition of Aβ aggregation, modulation of ChEs activity, and suppression of BACE1 and monoamine oxidase (MAO-A/B). Representative reported bioactive coumarins include AP2238 and S-14b,[13–16] and quinoline-based agents like tacrine, clioquinol (CQ), and tacrine-8-hydroxyquinoline hybrids (Fig. 1).[17–20] Additionally, both coumarin and quinoline scaffolds offer high synthetic tunability: the facile introduction of diverse substituents or linkers allows fine-tuning of lipophilicity, conformation, and interactions with target proteins, thereby enabling optimization of compounds' activity, selectivity, and

* Corresponding author.
E-mail addresses: chendaoyuan@zmuzh.edu.cn (D. Chen), xiachl@zmu.edu.cn (C. Xia).
[1] Shun Li and Xinrui Li contributed equally to this work.

https://doi.org/10.1016/j.bmc.2025.118499
Received 24 September 2025; Received in revised form 17 November 2025; Accepted 24 November 2025
Available online 26 November 2025

pharmacokinetic properties. Notably, many coumarin and quinoline derivatives exhibit favorable ADME profiles and blood-brain barrier (BBB) permeability, properties that are critical for achieving sufficient central nervous system exposure and therapeutic effect in AD. Theoretically, rationally combining these two scaffolds within a single molecule could preserve individual advantageous features while potentially generating synergistic effects that mitigate off-target effects and reduce the risk of resistance associated with single-target agents.

Considering the potential synergistic benefits of coupling coumarin and quinoline, here we undertook the rational design of a series of coumarin-quinoline hybrids, varying the linker length and sites between the two pharmacophores. This hybridization strategy aimed to develop MTDLs capable of simultaneously modulating multiple pathological hallmarks of AD (Fig. 2). A total of 24 coumarin-quinoline hybrids were synthesized via a streamlined two-step route and were then subjected to comprehensive in vitro inhibition evaluation against Aβ, ChE, and BACE1, alongside assessment of their BBB permeability using Parallel Artificial Membrane Permeation Assay (PAMPA). An optimal candidate, termed as **B8**, was selected for further mechanistic studies: its interaction with Aβ and its ability to protect SH-SY5Y cells from Aβ-induced cytotoxicity were examined. Finally, the in vivo efficacy of **B8** was assessed by behavioral testing and histopathological analysis of hippocampal neurons in an APP/PS1 transgenic AD mouse model.

2. Results and discussion

2.1. Chemistry

Coumarin and quinoline are renowned for their diverse biological activities and have individually been implicated in multiple facets of AD pathology.[21–24] To develop more potent multifunctional agents for AD treatment, we synthesized twenty-four novel coumarin-quinoline hybrids by varying the linker length, sites, and substituent groups. The synthesis of hybrids was achieved through two general methods: Scheme 1a was employed for **A1–A16** and Scheme 1b for **B1–B8**. The structures of compounds were characterized using ^{1}H NMR, ^{13}C NMR, and high-resolution mass spectrometry (HRMS), and their purities was confirmed to exceed 95 % through high-performance liquid chromatography (HPLC).

2.2. Screening of hybrids as multi-target-directed ligands

The inhibitory activity of compounds against $A\beta_{1-42}$ self-aggregation was assessed using the Thioflavin-T (ThT) fluorescence assay. As shown in Table 1, compared with the positive control resveratrol (res), most compounds exhibited moderate to strong inhibitory effects. Within series A, compounds with linker length n = 2 and n = 5 showed inhibition rates exceeding 40 %, which were higher than those observed for n = 3 and n = 4. While in series B, compounds with n = 2, 4, and 5 exhibited superior inhibitory activity compared with n = 3.

Subsequently, an initial in vitro screen for cholinesterase inhibition was performed using the Ellman's method.[25] At a test concentration of 5 μM, all compounds showed only weak inhibition of acetylcholinesterase (AChE). Therefore, IC_{50} and structure–activity relationship (SAR) analysis for AChE were not pursued. In contrast, the compounds displayed markedly different activities against butyrylcholinesterase (BuChE). Notably, **A4**, **B4**, and **B8** showed the most potent BuChE inhibition, with IC_{50} values of 0.1 μM, 4.9 μM, and 0.15 μM, respectively, indicating pronounced selectivity toward BuChE. Within series A, the combination of n = 5, R_1 = H, and R_2 = Cl, significantly enhanced BuChE activity. In series B, linker length emerged as a key determinant of BuChE potency, whereas the linker attachment site exerted only a minimal effect.

Taken together, compounds **A4**, **B4**, **B8** demonstrated a balanced profile of Aβ aggregation and BuChE inhibition and were therefore selected for further evaluation of BACE1 inhibition and BBB permeability. Using a FRET-based assay,[26] all tested compounds showed comparable BACE1 inhibitory activity at 10 μM (Table 2). Given the imperative of CNS exposure for AD therapeutics, BBB permeability was assessed by the PAMPA-BBB assay, with assay performance validated against 14 commercial reference drugs (Table S1 and Fig. S1). The PAMPA results (Table 2) indicated that both **B4** and **B8** could traverse the BBB.

Among all the compounds, **B8** displayed the most notable profile. Briefly, it inhibited $A\beta_{1-42}$ aggregation by 69.0 %, reduced BACE1 activity by 47.1 % at 10 μM, and potently inhibited BuChE with an IC_{50} of 0.15 μM. These combined properties, together with the favorable BBB permeability, identifying **B8** as the lead candidate for further investigation.

2.3. *B8* binds $A\beta_{1-42}$ with higher affinity than res

The binding affinity of **B8** to $A\beta_{1-42}$ was quantified using Surface Plasmon Resonance (SPR), after immobilizing $A\beta_{1-42}$ on a GLH senor chip. As depicted in Fig. 3, compared with res, **B8** displays a slow-on and slow-off binding mode with $A\beta_{1-42}$ and produces a higher signal intensity at equivalent concentrations. Fitting of the binding response yielded an equilibrium dissociation constant (K_D) of 4.38×10^{-5} M for the **B8**-$A\beta_{1-42}$ interaction, versus 1.78×10^{-4} M for Res, indicating that **B8** binds Aβ with substantially higher affinity than res.

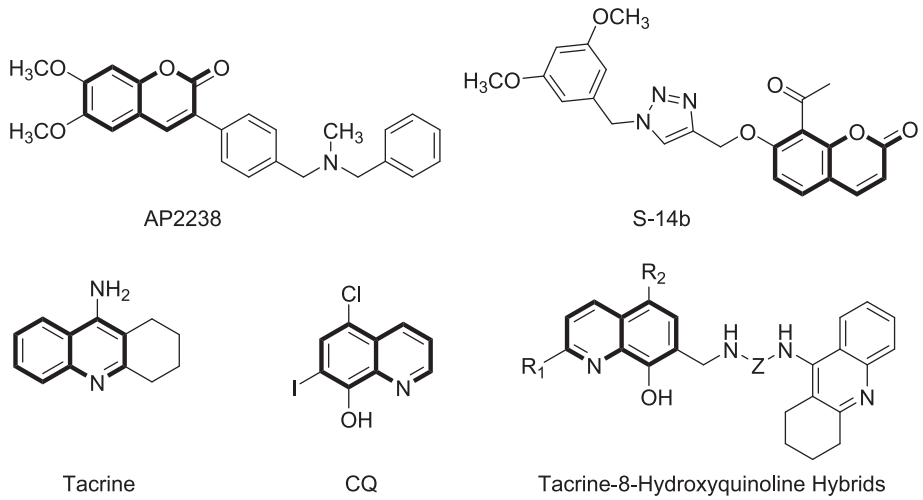

Fig. 1. Chemical structures of AP2238, S-14b, tacrine, clioquinol (CQ), and tacrine-8-hydroxyquinoline hybrids.

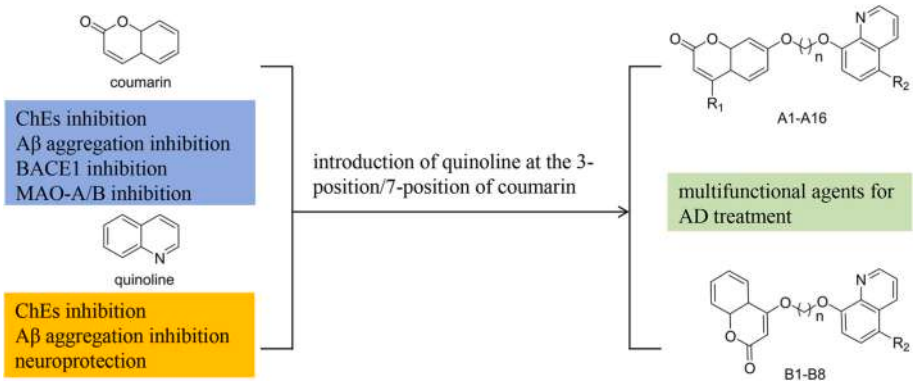

Fig. 2. Design strategies for new compounds **A1**–**A16** and **B1**–**B8.**

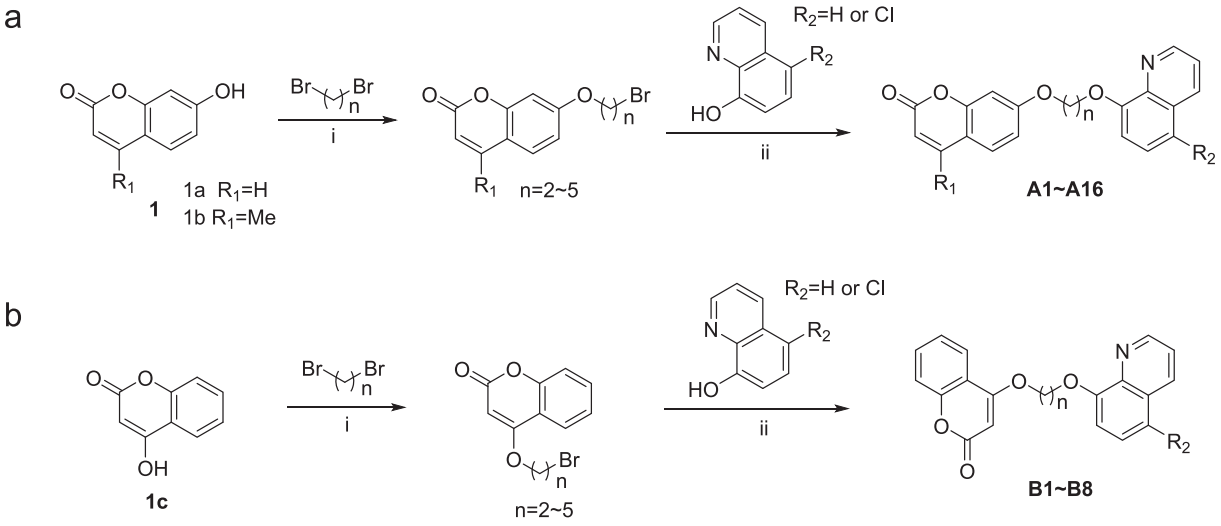

Scheme 1. Synthesis of Coumarin-Quinoline hybrids, reagents and conditions: (i) acetone, reflux, K_2CO_3, 2 h; (ii) MeCN, reflux, K_2CO_3, 2 h.

2.4. *B8 attenuated aβ-induced toxicity in SH-SY5Y neuronal cells*

The cytotoxicity of **B8** toward neuronal cells was evaluated using the MTT assay. As shown in Fig. 4A, **B8** displayed low neurotoxicity with an IC_{50} of 41.3 μM. In addition, no significant damage effect on the morphology of the SH-SY5Y cells were observed with concentrations below 10 μM (Fig. 4B).

Given the well-established role of toxic Aβ in inducing oxidative stress and apoptosis in neurons. Aβ-induced cell death in SH-SY5Y is a widely used model to study protective effect of candidate compounds.[8,27] As illustrated in Fig. 4C, approximately 48 % of SH-SY5Y cells underwent cell death when exposed to Aβ, while co-treatment with increasing concentrations of **B8** conferred dose-dependent protection against Aβ-induced cell death.

The protective effect of **B8** was further validated by flow cytometry. **B8** significantly mitigated oxidative stress and reduced the apoptotic rate in Aβ-induced SH-SY5Y cells (Fig. 4D and E). This observed neuroprotective effect theoretically may be attributed to the binding of **B8** to Aβ, neutralizing its cytotoxicity and thus attenuating oxidative damage and apoptosis.

2.5. *B8 treatment improves cognitive function and spatial memory in APP/PS1 mice*

The acute toxicity of **B8** was initially evaluated in Kunming mice using the up-and-down method. During the two-week oral administration, no signs of acute toxicity (including mortality, significant body weight loss, or alterations in food and water intake) were observed in the **B8**-treated groups. **B8** demonstrated an excellent safety profile, with a maximum tolerated oral dose of 2000 mg/kg. Following the two-week oral administration, the mice were euthanized and necropsy of major organs (heart, liver, spleen, lungs, and kidneys) revealed no visible damage attributable to **B8**.

The Morris water maze (MWM) test was utilized to evaluate the effect of **B8** (10 mg/kg/day) on learning and memory in APP/PS1 mice, with donepezil (2 mg/kg/day) serving as a positive control.[28] As depicted in Fig. 5A, during the five-day place navigation test, all experimental mice exhibited a gradual decrease in escape latency with increasing training days. However, when compared to the AD group, the WT (wild-type), Donepezil, and **B8** groups exhibited significantly shorter escape latency and search distance to locate the hidden platform. Notably, **B8**-treated mice displayed escape latency and search strategies comparable to WT mice with high spatial navigation efficiency (Fig. 5A, B). The findings suggest that **B8** treatment markedly enhances the spatial learning capabilities of AD model mice, approaching normal levels. Additionly, the mean swimming speed exhibited no significant differences across the groups (Fig. 5C), indicating that prolonged **B8** administration did not affect locomotor and exploratory behaviors in mice.

A spatial probe test was performed 24 h after completion of the place-navigation training. Compared with the AD group, **B8**-treated mice showed a marked increase in the number of platform crossings (Fig. 5D). Additionally, there was a significant increase in the percentage of path length and time spent in the target quadrant (Fig. 5E, F) as

Table 1
Inhibitory activity of Coumarin-Quinoline hybrids on Aβ aggregation, *h*AChE and *h*BuChE.

Cpds.	n	R_1	R_2	$A\beta_{1-42}$ aggregation inhibition (%)[a]	IC_{50} for *h*AChE[b]	IC_{50} for *h*BuChE[b]
A1	2	H	Cl	42.7 ± 0.2	>5(36.9 %)[c]	>5(29.0 %)[c]
A2	3	H	Cl	21.9 ± 2.7	>5(9.2 %)[c]	>5(12.0 %)[c]
A3	4	H	Cl	34.4 ± 0.5	>5(7.1 %)[c]	>5(14.1 %)[c]
A4	5	H	Cl	54.0 ± 3.3	>5(6.7 %)[c]	0.1 ± 0.0
A5	2	Me	Cl	46.6 ± 3.4	>5(7.9 %)[c]	>5(28.6 %)[c]
A6	3	Me	Cl	15.4 ± 2.5	>5(1.9 %)[c]	>5(39.5 %)[c]
A7	4	Me	Cl	35.6 ± 2.2	>5(7.1 %)[c]	>5(19.0 %)[c]
A8	5	Me	Cl	51.1 ± 3.8	>5(3.0 %)[c]	>5(18.5 %)[c]
A9	2	H	H	53.0 ± 1.4	>5(7.1 %)[c]	>5(25.7 %)[c]
A10	3	H	H	24.7 ± 2.3	>5(8.4 %)[c]	>5(14.7 %)[c]
A11	4	H	H	28.3 ± 1.5	>5(12.5 %[c]	>5(29.7 %)[c]
A12	5	H	H	47.9 ± 1.6	>5(21.0 %)[c]	>5(21.5 %)[c]
A13	2	Me	H	40.2 ± 1.2	>5(10.0 %)[c]	>5(22.8 %)[c]
A14	3	Me	H	29.9 ± 1.8	>5(12.0 %)[c]	>5(14.1 %)[c]
A15	4	Me	H	37.7 ± 1.3	>5(18.0 %)[c]	>5(25.8 %)[c]
A16	5	Me	H	46.4 ± 3.0	>5(44.4 %)[c]	>5(10.3 %)[c]
B1	2	–	Cl	48.2 ± 0.5	>5(4.5 %)[c]	>5(13.0 %)[c]
B2	3	–	Cl	4.4 ± 0.8	>5(7.0 %)[c]	>5(14.2 %)[c]
B3	4	–	Cl	50.7 ± 0.8	>5(8.8 %)[c]	>5(24.5 %)[c]
B4	5	–	Cl	52.1 ± 0.7	>5(5.3 %)[c]	4.9 ± 0.5
B5	2	–	H	49.4 ± 1.3	>5(2.7 %)[c]	>5(27.3 %)[c]
B6	3	–	H	19.0 ± 1.7	>5(7.2 %)[c]	>5(37.5 %)[c]
B7	4	–	H	42.3 ± 2.1	>5(6.5 %)[c]	>5(17.9 %)[c]
B8	5	–	H	69.0 ± 1.8	>5(20.8 %)[c]	0.15 ± 0.0
res				61.2 ± 4.8	n.d.[d]	n.d.[d]
Donepezil				n.d.[d]	0.03 ± 0.0	>5(29.3 %)
Tacrine				n.d.[d]	0.3 ± 0.1	0.02 ± 0.0

[a] The thioflavin-T fluorescence assay was employed to assess the inhibitory capacity of Aβ self-aggregation. Results are presented as the mean ± SD from a minimum of three independent experiments. All tests were conducted with 10 μM compounds and 25 μM $A\beta_{42}$, respectively.
[b] IC_{50}, the concentration of compounds that inhibited 50 % enzyme activity. The values are expressed as the mean ± SD of at least three independent experiments.
[c] The inhibitory activity of ChEs at the concentration of 5 μM.
[d] n.d., Not determined.

well as the virtual platform zone (Fig. 5G, H). Representative swim trajectories (Fig. 5I) provided further support for these findings: AD mice displayed random swimming patterns consistent with impaired memory retention, while Donepezil-treated mice concentrated exploration in the target quadrant. Notably, **B8**-treated mice exhibited focused searches and a strong preference for the target quadrant, with spatial memory performance comparable to WT animals. These results indicate that **B8** substantially improves spatial memory and cognitive function in APP/PS1 mice.

Table 2
Inhibitory activity on BACE1 and membrane permeability of selected hybrids **A4**, **B4** and **B8.**

Cpds.	BACE1 (%) [a]	$P_e(\times 10^{-6}$ cm/s) [b]	Prediction
A4	57.6 %	0.8 ± 0.1	CNS-
B4	48.9 %	13.6 ± 0.8	CNS+
B8	47.1 %	12.4 ± 0.7	CNS+
Positive control	96.4 %	n.d.[c]	n.d.[c]

[a] evaluate the BACE1 inhibitory activity, the concentration of compounds is 10 μM.
[b] Compounds with permeabilities $P_e > 3.8 \times 10^{-6}$ cm/s could cross the BBB, CNS+, high brain penetration; CNS−, low brain penetration.
[c] n.d., Not determined.

2.6. *B8 treatment protects against neuronal damage in APP/PS1 mice*

To investigate the pathological basis for the cognitive improvements observed in vivo, hematoxylin–eosin (HE) staining was performed to directly assess the neuronal degeneration in the hippocampus and cortex. As shown in Fig. 6A, WT mice exhibited well-organized, intact neurons, whereas saline-treated APP/PS1 mice displayed classic neuropathological features, including marked neuronal loss, nuclear pyknosis, and disrupted neuronal architecture. Conversely, treatment with **B8** or donepezil-treated markedly attenuated these pathological, neuronal organization and density were largely preserved and not significantly different from WT mice. Quantitative analysis of the degenerative cell index confirmed a significant reduction in necrotic pyramidal neurons in the cortex and hippocampal subfields (CA1, CA3, and DG) of **B8**-treated mice, an effect comparable to that of donepezil (Fig. 6B). These findings link the behavioral improvements produced by **B8** with its neuroprotective effects in critical memory circuits.

2.7. *B8 treatment reduces aβ burden in the brains of APP/PS1 mice*

To further elucidate the mechanism underlying **B8**'s neuroprotective effects, we assessed its impact on Aβ plaque burden, the primary and central pathological hallmark of AD. Immunohistochemical analysis revealed that **B8** treatment exhibited a significant reduction in both the size and density of Aβ plaques in the hippocampus compared with untreated AD mice (Fig. 7A). Notably, Quantification showed that the magnitude of Aβ clearance in the **B8** group was comparable to that observed with donepezil (Fig. 7B). These in vivo findings provide crucial evidence that **B8**'s therapeutic benefit shall be mediated by direct reduction of Aβ aggregation and deposition, a disease-modifying mechanism that is consistent with our in vitro results.

2.8. *B8 treatment attenuates oxidative stress and inflammatory response in APP/PS1 mice*

We next examined the effect of **B8** on oxidative stress and neuroinflammation, two key mediators of Aβ-induced neurotoxicity.[29,30] Biochemical assays in hippocampus and cortex showed that APP/PS1 mice displayed pronounced oxidative stress relative to WT, characterized by significantly reduced superoxide dismutase (SOD) activity and glutathione (GSH) levels, together with increased malondialdehyde (MDA) accumulation. **B8** treatment substantially ameliorated these disturbances: SOD activity and GSH levels were significantly increased while MDA content was reduced, indicating effective attenuation of oxidative damage (Fig. 8A-F). In parallel, the neuroinflammation was assessed by measuring pro-inflammatory cytokines IL-1β and TNF-α. Both cytokines were elevated in AD mice and were significantly downregulated by **B8** in cortex and hippocampus (Fig. 8G, H).

These findings suggest that the neuroprotective activity of **B8** is multi-faceted. **B8** directly targets the Aβ cascade by reducing its production via BACE1 inhibition and disrupting its aggregation, this action that mitigates a primary driver of AD pathogenesis: neuroinflammation

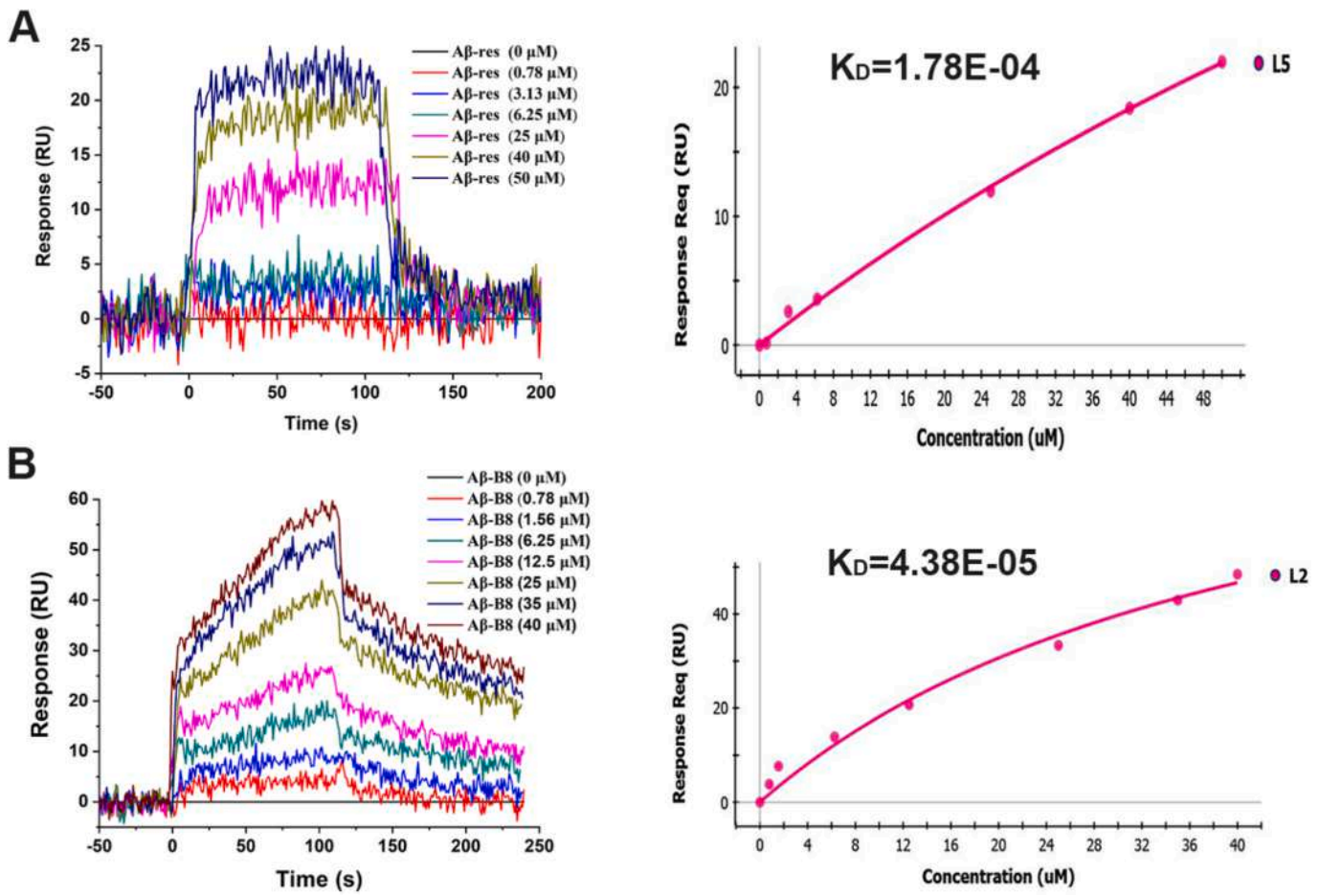

Fig. 3. SPR was utilized to examine the binding interaction between res (A) or **B8** (B) and $A\beta_{1-42}$. The equilibrium dissociation constant (K_D) for the interaction between res and $A\beta_{1-42}$ was determined to be 1.78×10^{-4} mol/L. The K_D for the interaction between **B8** and $A\beta_{1-42}$ was determined to be 4.38×10^{-5} mol/L.

and oxidative stress. Meanwhile, by inhibiting BuChE activity, it further suppresses the inflammatory cascade. Collectively, these synergistic actions on distinct pathological pathways underpin the comprehensive neuroprotection observed.

3. Conclusion

Although multi-target strategies hold considerable promise, their development and execution present significant challenges. The pharmacokinetics and pharmacodynamics of MTDLs are intricate, requiring rigorous clinical trials to establish their safety and efficacy. Moreover, identifying the optimal combination of pathophysiological targets and the most potent agents remains a major scientific challenge.[31] The coumarin-quinoline hybrid approach employed in this study provides a promising strategy to address these complexities. Specifically, the direct hybridization of coumarin and quinoline scaffolds remains a largely underexplored strategy. As a representative of this series, **B8** distinguishes itself from many recent MTDLs (Table S2)[5,14,32–35] through its multifaceted mechanism: it reduces upstream Aβ production via BACE1 inhibition, subsequently inhibits the aggregation of remaining Aβ peptide, and modulates the cholinergic system through potent BuChE inhibition, thereby collectively reducing downstream neuroinflammation and oxidative stress. Most importantly, this integrated multi-target profile was successfully translated into significant in vivo efficacy, culminating in robust neuroprotection and marked amelioration of cognitive impairment in APP/PS1 mice. Collectively, these findings indicate that **B8** exerts broad neuroprotective and disease-modifying effects via synergistic modulation of interconnected AD pathological pathways, highlighting the potential of coumarin-quinoline hybrids as a novel class of AD therapeutics.

4. Experimental section

4.1. Synthesis and characterization

All commercial chemicals used as starting materials were analytical grade and utilized without further purification. 600Mhz ^{1}HNMR and 151Mhz ^{13}CNMR spectra were recorded using TMS as the internal standard in DMSO-d_6 with a Bruker BioSpin GmbH spectrometer; Chemical shifts are reported in parts per million (ppm) relative to residual DMSO-d_6 (δ = 2.50,^{1}H; δ = 40.42–39.58,^{13}C) and $CDCl_3$ (δ = 7.26, ^{1}H; δ = 77.32–76.81, ^{13}C). Mass spectra (MS) were recorded on a Shimadzu LCMS-2010 A instrument with an ESI or ACPI mass selective detector, and high-resolution mass spectra (HRMS) on Shimadzu LCMS-IT-TOF. The purities of synthesized compounds were confirmed to be higher than 95 % by analytical HPLC performed with a dual pump Shimadzu LC-20AB system equipped with an Ultimate XB-C18 column and eluted with acetonitrile-water containing 0.1 % TFA. All the reagents were commercially available.

4.2. General procedure for the synthesis of *A1* ~ *A16* and *B1* ~ *B8*

4.2.1. Preparation of intermediates

In a 100 mL round-bottomed flask, 4-methylumbelliferone or 7-hydroxycoumarin (2 g, 12.34 mmol), K_2CO_3 (5.11 g, 37 mmol), the corresponding bromoethane (6.38 mL, 74.04 mmol) and 20 mL of

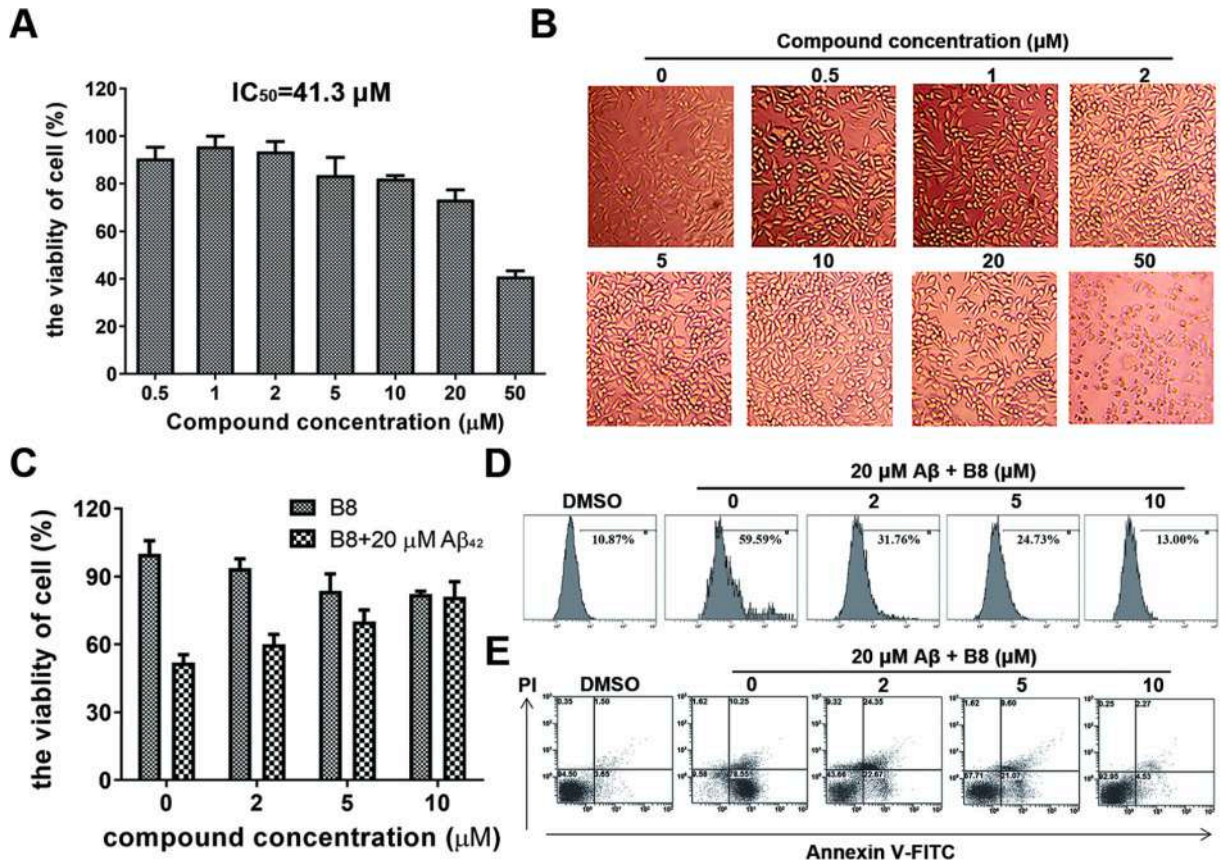

Fig. 4. The neuroprotective effect of **B8** against Aβ-induced damage in SH-SY5Y cells was evaluated. (A) The cells were treated with different concentrations of **B8** for a duration of 48 h, after which cell viability was assessed utilizing an MTT assay ($n = 3$). (B) The impact of the treatments was further examined through phase-contrast imaging after exposing the cells to varying concentrations of **B8** for 48 h. (C) Cells were pre-incubated with different concentrations of **B8** for 30 min, followed by exposure to 20 μM Aβ for 24 h. Afterwards, an MTT assay was employed to assess cell viability. All experiments were performed in three replicates. (D) The generation of ROS in SH-SY5Y cells was assessed through the analysis of dichlorofluorescein (DCF) fluorescence intensity using FACS. This evaluation was conducted 10 h following treatment with **B8** and Aβ at a concentration of 20 μM. (E) The prevention of Aβ-induced apoptosis in SH-SY5Y cells by **B8** was evaluated. Cells were pretreated with varying concentrations of **B8** for 30 min before being exposed to 20 μM of Aβ for 24 h, with a control group receiving no **B8** pretreatment. Apoptosis was subsequently quantified by flow cytometry using Annexin V-FITC/PI staining in the SH-SY5Y cells.

acetone were added, the mixture was heated to reflux. After completion, acetone was removed by rotary evaporation under reduced pressure. Then, 50 mL of water was added, and the mixture was thoroughly stirred and subjected to suction filtration. The filter cake was air-dried and further purified by silica gel column chromatography, yielding a white solid compound.

4.2.2. General synthesis procedure of hybrids

In a 50 mL round-bottomed flask equipped with a magnetic stir bar 8-hydroxyquinoline or 5-chloro-8-hydroxyquinoline (0.13 g, 0.74 mmol) and K_2CO_3 (0.20 g, 1.48 mmol) were suspended in acetonitrile (10 mL) and the mixture was heated to reflux. After 30 min, the corresponding intermediate (0.20 g, 0.74 mmol) was added, and the reflux was continued until the reaction completion. Acetonitrile was then removed by rotary evaporation under reduced pressure. Subsequently, 50 mL of water was added, and the mixture was thoroughly stirred and subjected to suction filtration. The filter cake was air-dried and further purified by silica gel column chromatography, resulting in a white solid compound.

4.2.3. 7-(2-((5-Chloroquinolin-8-yl) oxy) ethoxy)-2H-chromen-2-one (A1)

^{1}HNMR (600 MHz, DMSO-d_6) δ 8.96 (dd, J = 4.1, 1.6 Hz, 1H), 8.51 (dd, J = 8.5, 1.6 Hz, 1H), 8.01 (d, J = 9.5 Hz, 1H), 7.75–7.70 (m, 2H), 7.65 (d, J = 8.6 Hz, 1H), 7.30 (d, J = 8.5 Hz, 1H), 7.15 (d, J = 2.4 Hz, 1H), 7.03 (dd, J = 8.6, 2.4 Hz, 1H), 6.31 (d, J = 9.5 Hz, 1H), 4.60–4.56 (m, 4H). ^{13}CNMR (151 MHz, DMSO-d_6) δ 161.98, 160.78, 155.88, 154.13, 150.30, 144.81, 140.64, 132.69, 130.01, 127.30, 126.68, 123.58, 121.57, 113.37, 113.13, 113.04, 110.37, 101.96, 67.83, 67.69. HRMS (ESI): calcd for $C_{20}H_{14}ClNO_4$ $[M + H]^+$ 368.0684, found $[M + H]^+$ 368.0688. HPLC: tR =14.725 min (100.00 %).

4.2.4. 7-(3-((5-Chloroquinolin-8-yl) oxy) propoxy)-2H-chromen-2-one (A2)

^{1}HNMR (600 MHz, DMSO-d_6) δ 8.98 (dd, $J = 4.1$, 1.6 Hz, 1H), 8.50 (dd, $J = 8.5$, 1.6 Hz, 1H), 7.98 (d, $J = 9.5$ Hz, 1H), 7.72 (dd, $J = 8.5$, 4.1 Hz, 1H), 7.68 (d, $J = 8.4$ Hz, 1H), 7.62 (d, $J = 8.6$ Hz, 1H), 7.26 (d, $J = 8.5$ Hz, 1H), 7.04 (d, $J = 2.5$ Hz, 1H), 6.99 (dd, $J = 8.6$, 2.4 Hz, 1H), 6.28 (d, $J = 9.5$ Hz, 1H), 4.38–4.33 (m, 4H), 2.35 (p, $J = 6.2$ Hz, 2H). ^{13}C NMR (151 MHz, DMSO-d_6) δ 162.19, 160.69, 155.87, 154.30, 150.30, 144.79, 140.75, 132.66, 130.00, 127.31, 126.65, 123.53, 121.24, 113.19, 112.99, 112.89, 110.20, 101.78, 65.67, 65.62, 28.89. HRMS (ESI): calcd for $C_{21}H_{16}ClNO_4$ $[M + H]^+$ 382.0841, found $[M + H]^+$ 382.0613. HPLC: tR = 5.987 min (99.49 %).

4.2.5. 7-(4-((5-Chloroquinolin-8-yl) oxy) butoxy)-2H-chromen-2-one (A3)

^{1}HNMR (600 MHz, DMSO-d_6) δ 8.97 (dd, $J = 4.2$, 1.6 Hz, 1H), 8.49 (dd, $J = 8.5$, 1.6 Hz, 1H), 7.98 (d, $J = 9.5$ Hz, 1H), 7.71 (dd, $J = 8.5$, 4.1 Hz, 1H), 7.68 (d, $J = 8.4$ Hz, 1H), 7.61 (d, $J = 8.6$ Hz, 1H), 7.22 (d, $J = 8.5$ Hz, 1H), 7.00 (d, $J = 2.4$ Hz, 1H), 6.95 (dd, $J = 8.6$, 2.4 Hz, 1H), 6.28 (d, $J = 9.5$ Hz, 1H), 4.28–4.23 (m, 4H), 2.05–1.99 (m, 4H). ^{13}CNMR (151 MHz, DMSO-d_6) δ 162.33, 160.79, 155.88, 154.42, 150.22,

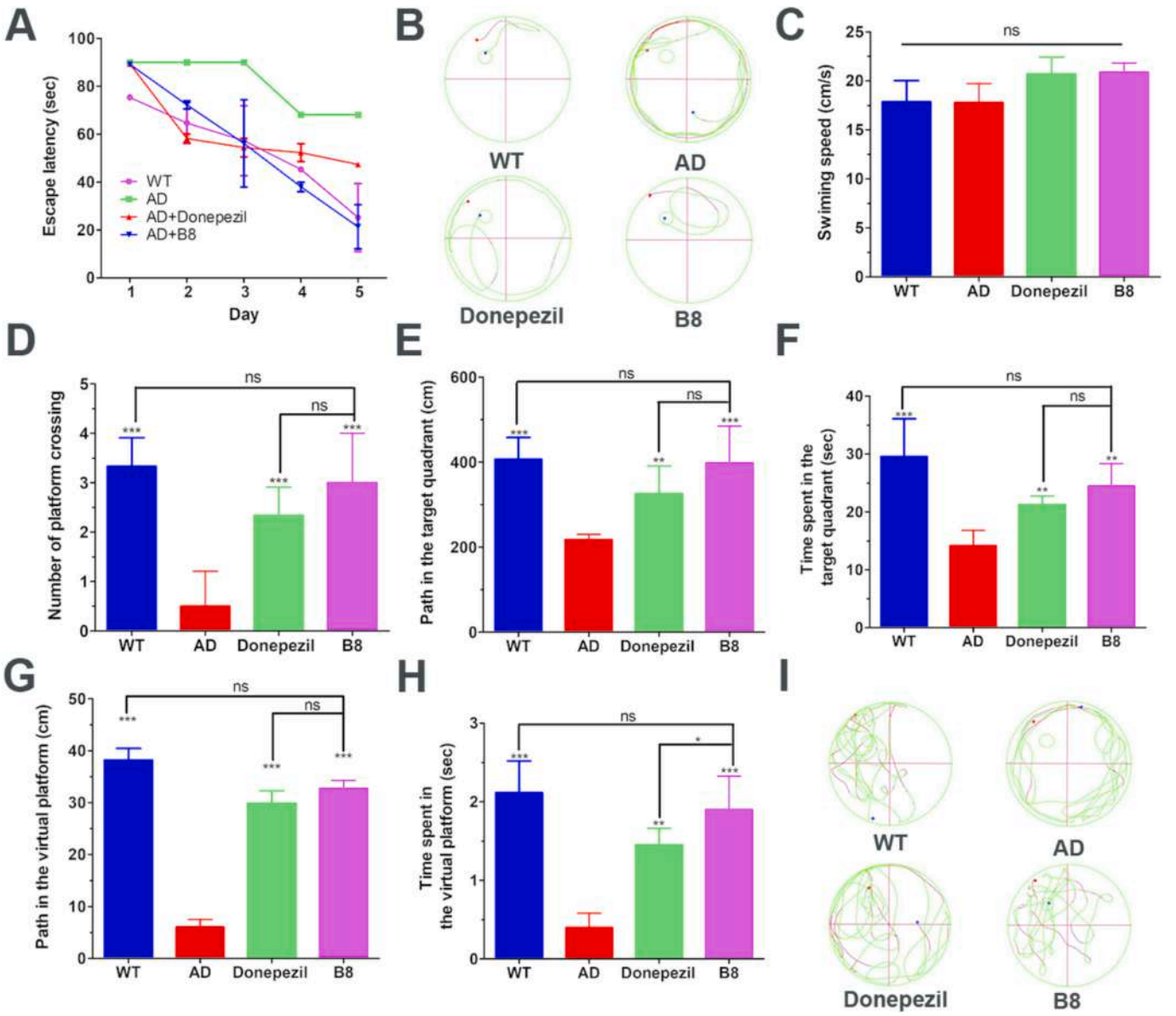

Fig. 5. B8 improves the cognitive ability and spatial memory of AD mice in MWM test ($n = 8$ mice/group). (A) The latency period for each group of experimental mice to locate hidden platforms during training; (B) Each group of mice's representative trajectories during their training in Morris water maze.; (C) The mean velocity of each experimental mouse group; (D) Times of crossing the virtual platform; The distance (E) and time (F) spent in the target quadrant; The distance (G) and time (H) spent in the virtual platform; (I) The representative track map of each group of experimental mice in the spatial probe test. One-way ANOVA followed by Newman−Keuls post hoc test, (ns) $p > 0.05$, (*) $p < 0.05$, (**) $p < 0.01$, (***) $p < 0.001$.

144.83, 140.75, 132.63, 129.91, 127.32, 126.63, 123.47, 120.98, 113.20, 112.86, 112.73, 109.94, 101.64, 68.74, 68.61, 25.96, 25.65. HRMS (ESI): calcd for $C_{22}H_{18}ClNO_4$ $[M + H]^+$ 396.0997, found $[M + H]^+$ 396.1048. HPLC: tR = 6.281 min (99.50 %).

*4.2.6. 7-((5-((5-Chloroquinolin-8-yl) oxy) pentyl) oxy)-2H-chromen-2-one (**A4**)*

^{1}HNMR (600 MHz, DMSO-d_6) δ 8.96 (dd, $J = 4.1$, 1.7 Hz, 1H), 8.49 (dd, $J = 8.5$, 1.6 Hz, 1H), 7.98 (d, $J = 9.5$ Hz, 1H), 7.71 (dd, $J = 8.5$, 4.1 Hz, 1H), 7.67 (d, $J = 8.4$ Hz, 1H), 7.61 (d, $J = 8.6$ Hz, 1H), 7.21 (d, $J = 8.5$ Hz, 1H), 6.98 (d, $J = 2.4$ Hz, 1H), 6.94 (dd, $J = 8.6$, 2.5 Hz, 1H), 6.28 (d, $J = 9.5$ Hz, 1H), 4.21 (t, $J = 6.4$ Hz, 2H), 4.13 (t, $J = 6.4$ Hz, 2H), 1.94 (p, $J = 6.7$ Hz, 2H), 1.87 (p, $J = 6.7$ Hz, 2H), 1.69–1.64 (m, 2H). ^{13}CNMR (151 MHz, DMSO-d_6) δ 162.37, 160.79, 155.90, 154.53, 150.18, 144.82, 140.76, 132.60, 129.93, 127.32, 126.62, 123.46, 120.92, 113.20, 112.86, 112.72, 109.93, 101.62, 68.95, 68.74, 28.77, 28.65, 22.76. HRMS (ESI): calcd for $C_{23}H_{20}ClNO_4$ $[M + H]^+$ 410.1154, found $[M + H]^+$ 410.1165. HPLC: tR = 6.766 min (98.25 %).

*4.2.7. 7-(2-((5-Chloroquinolin-8-yl) oxy) ethoxy)-4-methyl-2H-chromen-2-one (**A5**)*

^{1}H NMR (600 MHz, DMSO-d_6) δ 8.96 (dd, $J = 4.1$, 1.6 Hz, 1H), 8.52 (dd, $J = 8.5$, 1.6 Hz, 1H), 7.72 (ddd, $J = 11.0$, 8.6, 4.9 Hz, 3H), 7.30 (d, $J = 8.5$ Hz, 1H), 7.14 (d, $J = 2.5$ Hz, 1H), 7.05 (dd, $J = 8.8$, 2.5 Hz, 1H), 6.23 (d, $J = 1.4$ Hz, 1H), 4.61–4.56 (m, 4H), 2.41 (d, $J = 1.3$ Hz, 3H). ^{13}CNMR (151 MHz, DMSO-d_6) δ 161.90, 160.65, 155.25, 154.14, 153.92, 150.32, 140.65, 132.71, 127.31, 127.01, 126.69, 123.60, 121.57, 113.82, 113.08, 111.77, 110.40, 101.99, 67.85, 67.67, 18.62. HRMS (ESI): calcd for $C_{21}H_{16}ClNO_4$ $[M + H]^+$ 382.0841, found $[M + H]^+$ 382.0820. HPLC: tR = 12.681 min (95.77 %).

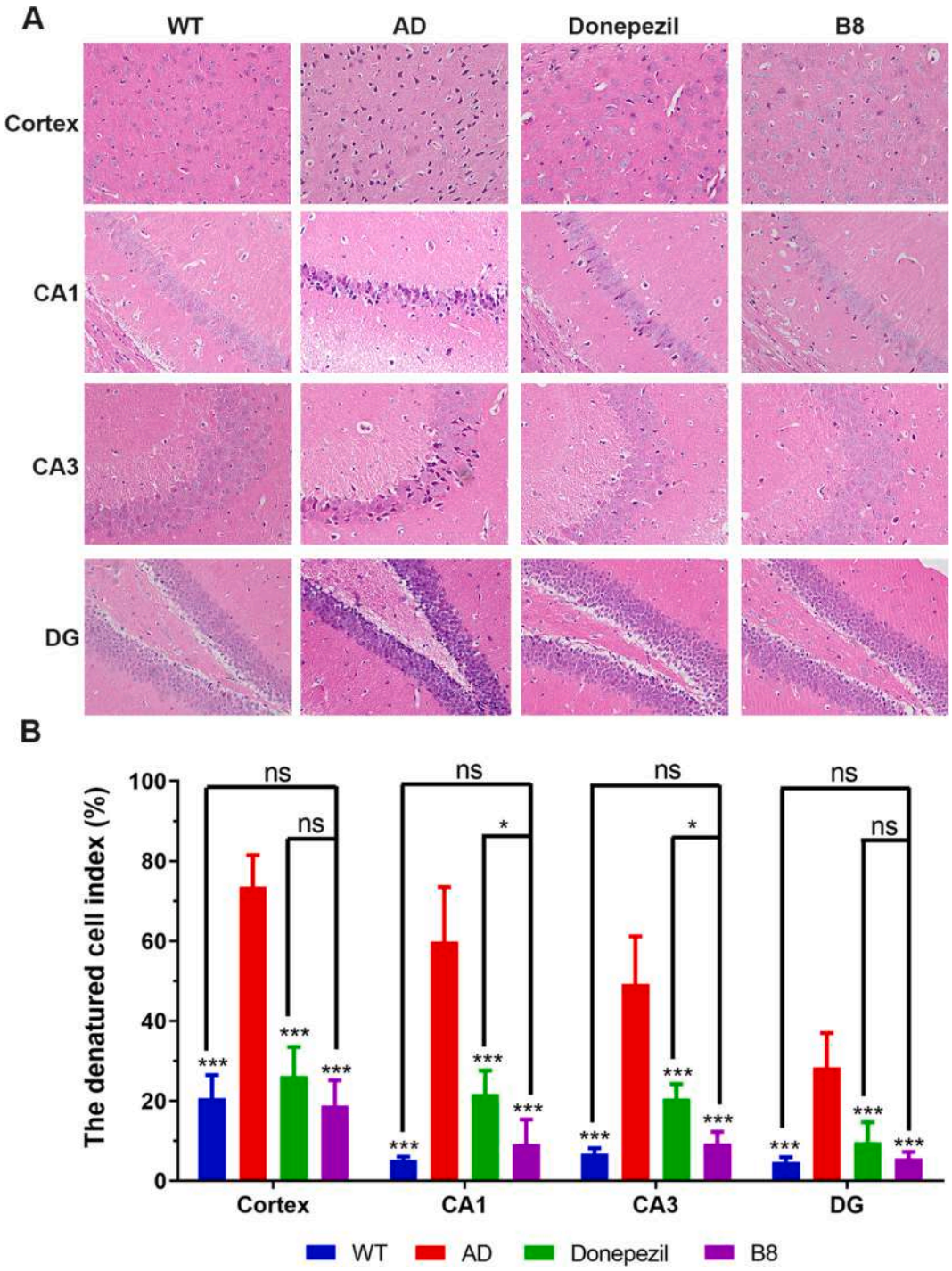

Fig. 6. HE staining was conducted on the cortex and hippocampal CA1, CA3, and DG regions of AD mice brains. (A) The representative images display the HE staining in the CA1, CA3 and DG regions of the hippocampus and cortex in the experimental mice (n = 4 mice/group), with a magnification of 200×. (B) The Denatured Cell Index (DCI), calculated as the number of denatured cells divided by the total number of cells, is presented for the mice's cortex and hippocampal neurons, The labels CA1, CA3, and DG denote the CA1, CA3, and DG regions of the hippocampus respectively. One-way ANOVA followed by Newman−Keuls post hoc test, (ns) $p > 0.05$, (*) $p < 0.05$, (**) $p < 0.01$, (***) $p < 0.001$.

*4.2.8. 7-(3-((5-Chloroquinolin-8-yl) oxy) propoxy)-4-methyl-2H-chromen-2-one (**A6**)*

^{1}HNMR (600 MHz, DMSO-d_6) δ 8.98 (dd, J = 4.2, 1.6 Hz, 1H), 8.49 (dd, J = 8.5, 1.7 Hz, 1H), 7.72 (dd, J = 8.5, 4.1 Hz, 1H), 7.68 (d, J = 8.4 Hz, 1H), 7.65 (d, J = 8.8 Hz, 1H), 7.25 (d, J = 8.4 Hz, 1H), 7.02 (d, J = 2.4 Hz, 1H), 6.99 (dd, J = 8.8, 2.5 Hz, 1H), 6.20 (d, J = 1.4 Hz, 1H), 4.36 (q, J = 6.4 Hz, 4H), 2.38 (d, J = 1.3 Hz, 3H), 2.37–2.33 (m, 2H). ^{13}CNMR (151 MHz, DMSO-d_6) δ 162.05, 160.61, 155.21, 154.31, 153.84, 150.30, 140.75, 132.64, 127.30, 126.93, 126.64, 123.51, 121.24, 113.64, 112.88, 111.64, 110.19, 101.78, 65.68, 65.60, 28.91, 18.57. HRMS (ESI): calcd for $C_{22}H_{18}ClNO_4$ $[M + H]^+$ 396.0997, found $[M + H]^+$ 396.0977. HPLC: tR = 6.241 min (99.66 %).

*4.2.9. 7-(4-((5-Chloroquinolin-8-yl) oxy) butoxy)-4-methyl-2H-chromen-2-one (**A7**)*

^{1}HNMR (600 MHz, DMSO-d_6) δ 8.97 (dd, J = 4.1, 1.6 Hz, 1H), 8.48

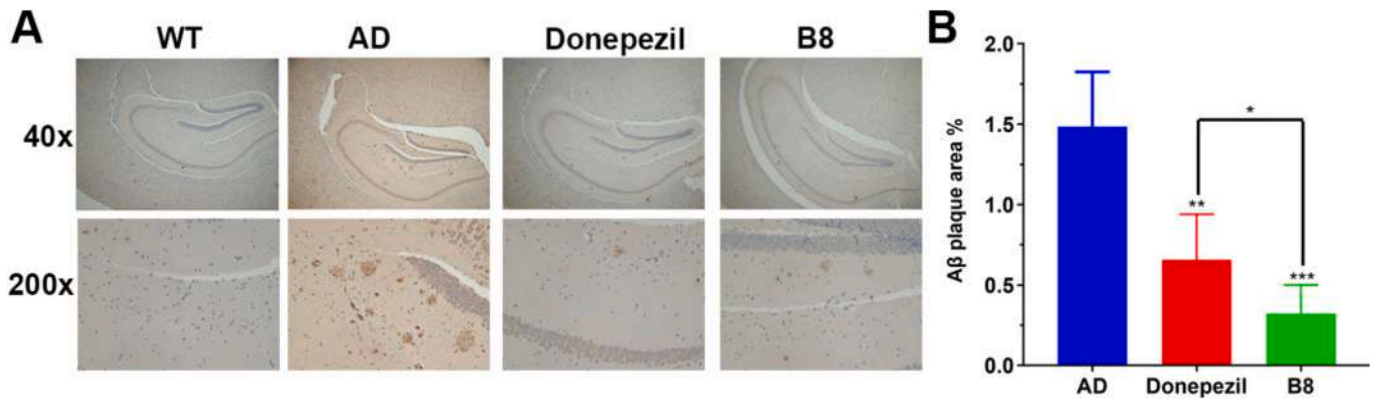

Fig. 7. B8 reduces Aβ burden in the brains of APP/PS1 mice. (A) Representative image of the Aβ immunoreactivity in the hippocampus of the experimental mice. (B) The percentage of plaque burden in the overall half-coronal hemisphere of the mice was analyzed and quantified using ImageJ software, expressed as the area of Aβ immunoreactivity relative to the full area ($n = 4$ mice/group). Values are expressed as mean ± SD, One-way ANOVA followed by Newman−Keuls post hoc test, (*) $p < 0.05$, (**) $p < 0.01$, (***) $p < 0.001$.

(dd, $J = 8.5$, 1.6 Hz, 1H), 7.70 (dd, $J = 8.5$, 4.1 Hz, 1H), 7.68 (d, $J = 8.4$ Hz, 1H), 7.64 (d, $J = 8.7$ Hz, 1H), 7.21 (d, $J = 8.4$ Hz, 1H), 6.98 (d, $J = 2.5$ Hz, 1H), 6.95 (dd, $J = 8.8$, 2.5 Hz, 1H), 6.20 (d, $J = 1.3$ Hz, 1H), 4.26 (dt, $J = 12.0$, 5.8 Hz, 4H), 2.39 (d, $J = 1.3$ Hz, 3H), 2.06–2.00 (m, 4H). ^{13}C NMR (151 MHz, DMSO-d_6) δ 162.20, 160.64, 155.20, 154.41, 153.88, 150.20, 140.74, 132.59, 127.30, 126.83, 126.62, 123.45, 120.98, 113.46, 112.91, 111.53, 109.91, 101.62, 68.74, 68.58, 25.95, 25.65, 18.58. HRMS (ESI): calcd for $C_{23}H_{20}ClNO_4$ $[M + H]^+$ 410.1154, found $[M + H]^+$ 410.1165. HPLC: tR = 6.508 min (99.29 %).

*4.2.10. 7-((5-((5-Chloroquinolin-8-yl) oxy) pentyl) oxy)-4-methyl-2H-chromen-2-one **(A8)***

^{1}H NMR (500 MHz, Chloroform-*d*) δ 9.01 (dd, $J = 4.2$, 1.6 Hz, 1H), 8.54 (dd, $J = 8.5$, 1.7 Hz, 1H), 7.56 (dd, $J = 8.5$, 4.2 Hz, 1H), 7.53 (d, $J = 8.4$ Hz, 1H), 7.47 (d, $J = 8.8$ Hz, 1H), 6.99 (d, $J = 8.4$ Hz, 1H), 6.84 (dd, $J = 8.8$, 2.5 Hz, 1H), 6.80 (d, $J = 2.5$ Hz, 1H), 6.13 (q, $J = 1.3$ Hz, 1H), 4.28 (t, $J = 6.7$ Hz, 2H), 4.07 (t, $J = 6.3$ Hz, 2H), 2.40 (d, $J = 1.3$ Hz, 3H), 2.15–2.09 (m, 2H), 1.95 (dt, $J = 14.8$, 6.5 Hz, 2H), 1.81–1.75 (m, 2H)·^{13}C NMR (126 MHz, $CDCl_3$) δ 162.09, 161.39, 155.26, 153.99, 152.61, 149.80, 140.86, 133.00, 127.11, 126.43, 125.49, 122.33, 122.06, 113.47, 112.57, 111.86, 108.54, 101.38, 68.93, 68.27, 28.80, 28.65, 22.74, 18.69. HRMS (ESI): calcd for $C_{24}H_{22}ClNO_4$ $[M + H]^+$ 424.1310, found $[M + H]^+$ 424.1326. HPLC: tR = 7.104 min (99.44 %).

*4.2.11. 7-(2-(Quinolin-8-yloxy) ethoxy)-2H-chromen-2-one **(A9)***

^{1}H NMR (600 MHz, DMSO-d_6) δ 8.86 (dd, $J = 4.1$, 1.7 Hz, 1H), 8.33 (dd, $J = 8.3$, 1.7 Hz, 1H), 8.01 (d, $J = 9.5$ Hz, 1H), 7.66 (d, $J = 8.6$ Hz, 1H), 7.56–7.51 (m, 3H), 7.28 (dd, $J = 6.7$, 2.2 Hz, 1H), 7.16 (d, $J = 2.4$ Hz, 1H), 7.04 (dd, $J = 8.6$, 2.4 Hz, 1H), 6.31 (d, $J = 9.5$ Hz, 1H), 4.60–4.57 (m, 2H), 4.56 (dd, $J = 6.3$, 2.9 Hz, 2H). ^{13}CNMR (151 MHz, DMSO-d_6) δ 162.06, 160.79, 155.91, 154.63, 149.50, 144.83, 140.14, 136.31, 130.03, 129.57, 127.30, 122.39, 120.54, 113.39, 113.12, 113.02, 110.26, 101.96, 67.82, 67.56. HRMS (ESI): calcd for $C_{20}H_{15}NO_4$ $[M + H]^+$ 334.1074, found $[M + H]^+$ 334.1146. HPLC: tR = 11.776 min (100.00 %).

*4.2.12. 7-(3-(Quinolin-8-yloxy) propoxy)-2H-chromen-2-one **(A10)***

^{1}HNMR (600 MHz, DMSO-d_6) δ 8.87 (dd, $J = 4.1$, 1.8 Hz, 1H), 8.31 (dd, $J = 8.3$, 1.8 Hz, 1H), 7.98 (d, $J = 9.5$ Hz, 1H), 7.62 (d, $J = 8.6$ Hz, 1H), 7.54 (dd, $J = 8.3$, 4.1 Hz, 1H), 7.51 (s, 1H), 7.50 (d, $J = 1.4$ Hz, 1H), 7.25 (dd, $J = 5.1$, 3.9 Hz, 1H), 7.05 (d, $J = 2.4$ Hz, 1H), 7.00 (dd, $J = 8.6$, 2.4 Hz, 1H), 6.29 (d, $J = 9.5$ Hz, 1H), 4.36 (td, $J = 6.2$, 4.7 Hz, 4H), 2.35 (p, $J = 6.2$ Hz, 2H). ^{13}CNMR (151 MHz, DMSO-d_6) δ 162.19, 160.78, 155.89, 154.80, 149.50, 144.80, 140.26, 136.27, 130.01, 129.52, 127.30, 122.33, 120.23, 113.19, 112.98, 112.89, 110.08, 101.79, 65.69, 65.33, 29.00. HRMS (ESI): calcd for $C_{21}H_{17}NO_4$ $[M + H]^+$ 348.1230, found $[M + H]^+$ 348.1230. HPLC: tR = 4.176 min (99.55 %).

*4.2.13. 7-(4-(Quinolin-8-yloxy) butoxy)-2H-chromen-2-one **(A11)***

^{1}HNMR (600 MHz, DMSO-d_6) δ 8.88 (dd, $J = 4.1$, 1.8 Hz, 1H), 8.30 (dd, $J = 8.3$, 1.8 Hz, 1H), 7.99 (d, $J = 9.4$ Hz, 1H), 7.62 (d, $J = 8.6$ Hz, 1H), 7.54 (dd, $J = 8.3$, 4.1 Hz, 1H), 7.52–7.47 (m, 2H), 7.21 (dd, $J = 6.4$, 2.6 Hz, 1H), 7.03 (d, $J = 2.4$ Hz, 1H), 6.97 (dd, $J = 8.6$, 2.4 Hz, 1H), 6.29 (d, $J = 9.4$ Hz, 1H), 4.26 (td, $J = 6.1$, 2.6 Hz, 4H), 2.05–2.00 (m, 4H). ^{13}CNMR (151 MHz, DMSO-d_6) δ 162.38, 160.80, 155.90, 154.95, 149.43, 144.83, 140.26, 136.25, 129.93, 129.52, 127.31, 122.28, 119.97, 113.22, 112.86, 112.73, 109.81, 101.66, 68.69, 68.45, 26.07, 25.79. HRMS (ESI): calcd for $C_{22}H_{19}NO_4$ $[M + H]^+$ 362.1387, found $[M + H]^+$ 362.1375. HPLC: tR = 4.386 min (98.61 %).

*4.2.14. 7-((5-(Quinolin-8-yloxy) pentyl) oxy)-2H-chromen-2-one **(A12)***

^{1}HNMR (600 MHz, DMSO-d_6) δ 8.85 (dd, $J = 4.1$, 1.8 Hz, 1H), 8.30 (dd, $J = 8.2$, 1.8 Hz, 1H), 7.98 (d, $J = 9.4$ Hz, 1H), 7.61 (d, $J = 8.6$ Hz, 1H), 7.53 (dd, $J = 8.3$, 4.1 Hz, 1H), 7.50–7.47 (m, 2H), 7.20 (dd, $J = 6.2$, 2.9 Hz, 1H), 6.99 (d, $J = 2.4$ Hz, 1H), 6.95 (dd, $J = 8.6$, 2.4 Hz, 1H), 6.28 (d, $J = 9.4$ Hz, 1H), 4.20 (t, $J = 6.4$ Hz, 2H), 4.13 (t, $J = 6.5$ Hz, 2H), 1.94 (p, $J = 6.6$ Hz, 2H), 1.87 (p, $J = 6.7$ Hz, 2H), 1.71–1.65 (m, 2H). ^{13}CNMR (151 MHz, DMSO-d_6) δ 162.39, 160.81, 155.91, 155.05, 149.37, 144.84, 140.28, 136.22, 129.94, 129.51, 127.32, 122.26, 119.91, 113.22, 112.86, 112.73, 109.81, 101.64, 68.78, 68.66, 28.93, 28.70, 22.84. HRMS (ESI): calcd for $C_{23}H_{21}NO_4$ $[M + H]^+$ 376.1543, found $[M + H]^+$ 376.1203. HPLC: tR = 4.726 min (99.73 %).

*4.2.15. 4-Methyl-7-(2-(quinolin-8-yloxy) ethoxy)-2H-chromen-2-one **(A13)***

^{1}H NMR (600 MHz, DMSO-d_6) δ 8.86 (dd, $J = 4.1$, 1.8 Hz, 1H), 8.33 (dd, $J = 8.2$, 1.8 Hz, 1H), 7.66 (d, $J = 8.6$ Hz, 1H), 7.57–7.52 (m, 3H), 7.29 (dd, $J = 6.7$, 2.3 Hz, 1H), 7.16 (d, $J = 2.5$ Hz, 1H), 7.04 (dd, $J = 8.6$, 2.5 Hz, 1H), 6.31 (d, $J = 9.4$ Hz, 1H), 4.61–4.58 (m, 2H), 4.57–4.55 (m, 2H), 2.42 (d, $J = 1.3$ Hz, 3H). ^{13}CNMR (151 MHz, DMSO-d_6) δ 162.06, 160.80, 155.91, 154.63, 149.50, 144.83, 140.14, 136.31, 130.03, 129.57, 127.30, 122.39, 120.55, 113.39, 113.12, 113.02, 110.26, 101.96, 67.82, 67.56, 18.62. HRMS (ESI): calcd for $C_{21}H_{17}NO_4$ $[M + H]^+$ 348.1230, found $[M + H]^+$ 348.1175. HPLC: tR = 4.080 min (99.66 %).

*4.2.16. 4-Methyl-7-(3-(quinolin-8-yloxy) propoxy)-2H-chromen-2-one **(A14)***

^{1}HNMR (600 MHz, DMSO-d_6) δ 8.87 (dd, $J = 4.1$, 1.8 Hz, 1H), 8.31 (dd, $J = 8.2$, 1.8 Hz, 1H), 7.67 (d, $J = 8.8$ Hz, 1H), 7.54 (dd, $J = 8.3$, 4.1 Hz, 1H), 7.51 (s, 1H), 7.50 (d, $J = 1.3$ Hz, 1H), 7.25 (dd, $J = 4.9$, 4.0 Hz, 1H), 7.04 (d, $J = 2.4$ Hz, 1H), 7.01 (dd, $J = 8.8$, 2.5 Hz, 1H), 6.20 (q, $J =$

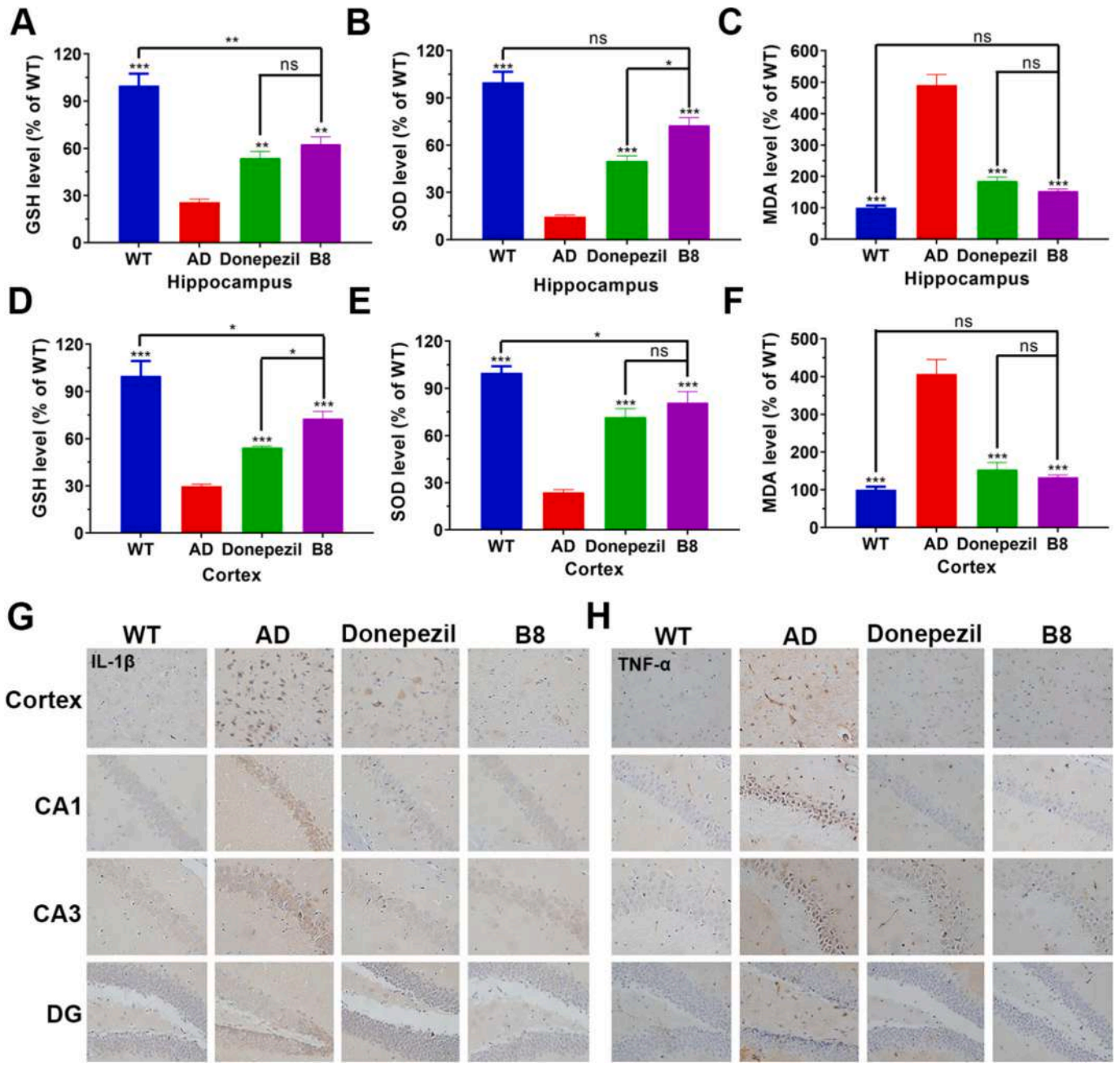

Fig. 8. The effects of **B8** on the levels of oxidative stress biomarkers GSH (A), SOD (B), and MDA (C) in the hippocampus and GSH (D), SOD (E), and MDA (F) in the cortex of AD mice ($n = 4$ mice/group). The immunohistochemical results of IL-1β (G) and TNFα (H) in the cortex and hippocampal CA1, CA3, and DG regions of AD mice brain ($n = 4$ mice/group). Values are expressed as mean ± SD, One-way ANOVA followed by Newman−Keuls post hoc test, (ns) $p > 0.05$, (*) $p < 0.05$, (**) $p < 0.01$, (***) $p < 0.001$.

1.3 Hz, 1H), 4.36 (q, $J = 6.1$ Hz, 4H), 2.39 (d, $J = 1.2$ Hz, 3H), 2.36 (q, $J = 6.2$ Hz, 2H). ^{13}CNMR (151 MHz, DMSO-d_6) δ 162.09, 160.63, 155.24, 154.81, 153.87, 149.50, 140.26, 136.27, 129.53, 127.30, 126.97, 122.33, 120.23, 113.65, 112.89, 111.64, 110.08, 101.81, 65.67, 65.34, 29.01, 18.58. HRMS (ESI): calcd for $C_{22}H_{19}NO_4$ $[M + H]^+$ 362.1387, found $[M + H]^+$ 362.1375. HPLC: tR = 4.431 min (99.37 %).

*4.2.17. 4-Methyl-7-(4-(quinolin-8-yloxy) butoxy)-2H-chromen-2-one (**A15**)*

^{1}HNMR (600 MHz, DMSO-d_6) δ 8.87 (dd, $J = 4.1$, 1.8 Hz, 1H), 8.30 (dd, $J = 8.2$, 1.8 Hz, 1H), 7.66 (d, $J = 8.8$ Hz, 1H), 7.53 (dd, $J = 8.3$, 4.1 Hz, 1H), 7.51–7.47 (m, 2H), 7.21 (dd, $J = 6.5$, 2.5 Hz, 1H), 7.01 (d, $J = 2.5$ Hz, 1H), 6.98 (dd, $J = 8.7$, 2.5 Hz, 1H), 6.20 (d, $J = 1.5$ Hz, 1H), 4.26 (q, $J = 5.8$ Hz, 4H), 2.39 (d, $J = 1.3$ Hz, 3H), 2.03 (qd, $J = 7.4$, 6.7, 3.2 Hz, 4H). ^{13}CNMR (151 MHz, DMSO-d_6) δ 162.27, 160.66, 155.25, 154.94, 153.92, 149.43, 140.26, 136.24, 129.52, 127.31, 126.89, 122.28, 119.97, 113.49, 112.94, 111.53, 109.81, 101.66, 68.66, 68.45, 26.06, 25.79, 18.60. HRMS (ESI): calcd for $C_{23}H_{21}NO_4$ $[M + H]^+$ 376.1543, found $[M + H]^+$ 376.1544. HPLC: tR = 4.564 min (99.27 %).

*4.2.18. 4-Methyl-7-((5-(quinolin-8-yloxy) pentyl) oxy)-2H-chromen-2-one (**A16**)*

^{1}HNMR (600 MHz, DMSO-d_6) δ 8.85 (dd, $J = 4.1$, 1.8 Hz, 1H), 8.30 (dd, $J = 8.3$, 1.8 Hz, 1H), 7.66 (d, $J = 8.7$ Hz, 1H), 7.53 (dd, $J = 8.3$, 4.1 Hz, 1H), 7.50–7.46 (m, 2H), 7.20 (dd, $J = 6.2$, 2.9 Hz, 1H), 6.98–6.95 (m, 2H), 6.20 (q, $J = 1.3$ Hz, 1H), 4.19 (t, $J = 6.4$ Hz, 2H), 4.14 (t, $J =$

6.5 Hz, 2H), 2.39 (d, J = 1.3 Hz, 3H), 1.94 (p, J = 6.6 Hz, 2H), 1.87 (p, J = 6.7 Hz, 2H), 1.71–1.65 (m, 2H). ^{13}CNMR (151 MHz, DMSO-d_6) δ 162.28, 160.66, 155.25, 155.04, 153.90, 149.37, 140.27, 136.22, 129.51, 127.32, 126.89, 122.25, 119.91, 113.48, 112.92, 111.53, 109.81, 101.65, 68.74, 68.65, 28.93, 28.71, 22.83, 18.58. HRMS (ESI): calcd for $C_{24}H_{23}NO_4$ $[M + H]^+$ 390.1700, found $[M + H]^+$ 390.1664. HPLC: tR = 5.031 min (99.33 %).

4.2.19. 4-(2-((5-Chloroquinolin-8-yl) oxy) ethoxy)-2H-chromen-2-one (B1)

^{1}HNMR (600 MHz, DMSO-d_6) δ 8.95 (dd, J = 4.1, 1.6 Hz, 1H), 8.52 (dd, J = 8.5, 1.6 Hz, 1H), 7.76–7.69 (m, 3H), 7.65 (ddd, J = 8.7, 7.3, 1.7 Hz, 1H), 7.40 (dd, J = 8.4, 1.0 Hz, 1H), 7.36 (d, J = 8.4 Hz, 1H), 7.31 (ddd, J = 8.1, 7.4, 1.1 Hz, 1H), 6.07 (s, 1H), 4.73–4.68 (m, 4H). ^{13}CNMR (151 MHz, DMSO-d_6) δ 165.23, 162.07, 154.18, 153.24, 150.40, 140.81, 133.29, 132.74, 127.29, 126.75, 124.62, 123.59, 123.37, 121.87, 116.94, 115.57, 111.16, 91.63, 68.92, 67.59. HRMS (ESI): calcd for $C_{20}H_{14}ClNO_4$ $[M + H]^+$ 368.0684, found $[M + H]^+$ 368.0620. HPLC: tR = 5.861 min (98.80 %).

4.2.20. 4-(3-((5-Chloroquinolin-8-yl) oxy) propoxy)-2H-chromen-2-one (B2)

^{1}HNMR (600 MHz, DMSO-d_6) δ 8.97 (dd, J = 4.2, 1.6 Hz, 1H), 8.49 (dd, J = 8.5, 1.7 Hz, 1H), 7.88 (dd, J = 7.8, 1.6 Hz, 1H), 7.72 (dd, J = 8.5, 4.1 Hz, 1H), 7.68 (d, J = 8.3 Hz, 1H), 7.64 (ddd, J = 8.7, 7.3, 1.6 Hz, 1H), 7.38 (dd, J = 8.4, 1.1 Hz, 1H), 7.30 (ddd, J = 8.1, 7.4, 1.1 Hz, 1H), 7.27 (d, J = 8.4 Hz, 1H), 5.96 (s, 1H), 4.48 (t, J = 6.0 Hz, 2H), 4.43 (t, J = 6.1 Hz, 2H), 2.45 (p, J = 6.1 Hz, 2H). ^{13}CNMR (151 MHz, DMSO-d_6) δ 165.42, 162.11, 154.31, 153.22, 150.28, 140.75, 133.19, 132.65, 127.30, 126.65, 124.55, 123.56, 123.53, 121.26, 116.84, 115.68, 110.25, 91.06, 67.14, 65.94, 28.48. HRMS (ESI): calcd for $C_{21}H_{16}ClNO_4$ $[M + H]^+$ 382.0841, found $[M + H]^+$ 382.0820. HPLC: tR = 6.088 min (99.86 %).

4.2.21. 4-(4-((5-Chloroquinolin-8-yl) oxy) butoxy)-2H-chromen-2-one (B3)

^{1}HNMR (600 MHz, DMSO-d_6) δ 8.96 (dd, J = 4.0, 1.6 Hz, 1H), 8.47 (dd, J = 8.5, 1.6 Hz, 1H), 7.74 (dd, J = 7.9, 1.6 Hz, 1H), 7.71 (dd, J = 8.5, 4.1 Hz, 1H), 7.66 (d, J = 8.4 Hz, 1H), 7.63 (ddd, J = 8.7, 7.3, 1.6 Hz, 1H), 7.37 (d, J = 8.4 Hz, 1H), 7.31–7.28 (m, 1H), 7.22 (d, J = 8.5 Hz, 1H), 5.94 (s, 1H), 4.41 (t, J = 5.9 Hz, 2H), 4.31 (t, 2H), 2.13–2.07 (m, 4H). ^{13}CNMR (151 MHz, DMSO-d_6) δ 164.36, 161.13, 153.25, 152.12, 149.13, 139.65, 132.05, 131.53, 126.21, 125.54, 123.49, 122.42, 122.15, 119.92, 115.79, 114.60, 108.85, 89.97, 68.79, 67.59, 24.54, 24.44. HRMS (ESI): calcd for $C_{22}H_{18}ClNO_4$ $[M + H]^+$ 396.0997, found $[M + H]^+$ 396.0977. HPLC: tR = 6.287 min (98.17 %).

4.2.22. 4-((5-((5-Chloroquinolin-8-yl) oxy) pentyl) oxy)-2H-chromen-2-one (B4)

^{1}HNMR (600 MHz, DMSO-d_6) δ 8.95 (dd, J = 4.1, 1.6 Hz, 1H), 8.49 (dd, J = 8.5, 1.7 Hz, 1H), 7.78 (dd, J = 7.9, 1.6 Hz, 1H), 7.71 (dd, J = 8.5, 4.2 Hz, 1H), 7.67 (d, J = 8.4 Hz, 1H), 7.66–7.63 (m, 1H), 7.39 (dd, J = 8.4, 1.1 Hz, 1H), 7.32–7.29 (m, 1H), 7.22 (d, J = 8.5 Hz, 1H), 5.90 (s, 1H), 4.27 (t, J = 6.3 Hz, 2H), 4.23 (t, J = 6.4 Hz, 2H), 1.99–1.93 (m, 4H), 1.76–1.70 (m, 2H). ^{13}C NMR (151 MHz, DMSO-d_6) δ 165.45, 162.16, 154.52, 153.24, 150.17, 140.77, 133.16, 132.60, 127.31, 126.63, 124.59, 123.45, 123.24, 120.92, 116.92, 115.75, 109.92, 90.98, 69.88, 68.85, 28.64, 28.13, 22.65. HRMS (ESI): calcd for $C_{23}H_{20}ClNO_4$ $[M + H]^+$ 410.1154, found $[M + H]^+$ 410.1094. HPLC: tR = 6.851 min (99.88 %).

4.2.23. 4-(2-(Quinolin-8-yloxy) ethoxy)-2H-chromen-2-one (B5)

^{1}HNMR (600 MHz, DMSO-d_6) δ 8.85 (dd, J = 4.1, 1.8 Hz, 1H), 8.33 (dd, J = 8.3, 1.8 Hz, 1H), 7.73 (dd, J = 7.9, 1.6 Hz, 1H), 7.65 (ddd, J = 8.5, 7.3, 1.6 Hz, 1H), 7.58–7.53 (m, 3H), 7.41 (dd, J = 8.4, 1.0 Hz, 1H), 7.35 (dd, J = 7.0, 1.9 Hz, 1H), 7.33–7.30 (m, 1H), 6.08 (s, 1H), 4.72 (dd, J = 6.2, 2.5 Hz, 2H), 4.69 (dd, J = 6.1, 2.5 Hz, 2H). ^{13}CNMR (151 MHz, DMSO-d_6) δ 165.28, 162.08, 154.67, 153.25, 149.58, 140.28, 136.35, 133.28, 129.62, 127.27, 124.62, 123.40, 122.38, 120.84, 116.92, 115.59, 110.99, 91.57, 69.05, 67.31. HRMS (ESI): calcd for $C_{20}H_{15}NO_4$ $[M + H]^+$ 334.1074, found $[M + H]^+$ 334.1039. HPLC: tR = 4.066 min (99.59 %).

4.2.24. 4-(3-(Quinolin-8-yloxy) propoxy)-2H-chromen-2-one (B6)

^{1}HNMR (600 MHz, DMSO-d_6) δ 8.87 (dd, J = 4.1, 1.8 Hz, 1H), 8.31 (dd, J = 8.3, 1.8 Hz, 1H), 7.90 (dd, J = 8.0, 1.6 Hz, 1H), 7.64 (ddd, J = 8.7, 7.3, 1.6 Hz, 1H), 7.54 (dd, J = 8.3, 4.1 Hz, 1H), 7.52–7.49 (m, 2H), 7.38 (dd, J = 8.4, 1.1 Hz, 1H), 7.31 (ddd, J = 8.2, 7.4, 1.1 Hz, 1H), 7.26 (dd, J = 5.2, 3.8 Hz, 1H), 5.97 (s, 1H), 4.49 (t, J = 6.0 Hz, 2H), 4.42 (t, J = 6.2 Hz, 2H), 2.45 (p, J = 6.1 Hz, 2H). ^{13}CNMR (151 MHz, DMSO-d_6) δ 165.45, 162.12, 154.80, 153.24, 149.49, 140.26, 136.28, 133.19, 129.54, 127.30, 124.59, 123.58, 122.33, 120.25, 116.84, 115.70, 110.13, 91.06, 67.18, 65.57, 28.60. HRMS (ESI): calcd for $C_{21}H_{17}NO_4$ $[M + H]^+$ 348.1230, found $[M + H]^+$ 348.1175. HPLC: tR = 4.274 min (99.70 %).

4.2.25. 4-(4-(Quinolin-8-yloxy) butoxy)-2H-chromen-2-one (B7)

^{1}HNMR (600 MHz, DMSO-d_6) δ 8.87 (dd, J = 4.1, 1.8 Hz, 1H), 8.30 (dd, J = 8.3, 1.8 Hz, 1H), 7.78 (dd, J = 7.9, 1.6 Hz, 1H), 7.64 (ddd, J = 8.7, 7.3, 1.6 Hz, 1H), 7.54 (dd, J = 8.3, 4.1 Hz, 1H), 7.51–7.48 (m, 2H), 7.39 (dd, J = 8.4, 1.1 Hz, 1H), 7.31 (ddd, J = 8.2, 7.3, 1.1 Hz, 1H), 7.21 (dd, J = 6.3, 2.7 Hz, 1H), 5.97 (s, 1H), 4.43 (t, J = 6.1 Hz, 2H), 4.29 (t, J = 5.9 Hz, 2H), 2.14–2.07 (m, 4H). ^{13}CNMR (151 MHz, DMSO-d_6) δ 165.49, 162.23, 154.87, 153.24, 149.45, 140.25, 136.24, 133.15, 129.52, 127.29, 124.60, 123.29, 122.31, 119.99, 116.90, 115.74, 109.79, 91.07, 69.97, 68.38, 25.72, 25.69. HRMS (ESI): calcd for $C_{22}H_{19}NO_4$ $[M + H]^+$ 362.1387, found $[M + H]^+$ 362.1375. HPLC: tR = 4.367 min (99.65 %).

4.2.26. 4-((5-(Quinolin-8-yloxy) pentyl) oxy)-2H-chromen-2-one (B8)

^{1}HNMR (600 MHz, DMSO-d_6) δ 8.84 (dd, J = 4.1, 1.7 Hz, 1H), 8.30 (dd, J = 8.3, 1.8 Hz, 1H), 7.80 (dd, J = 7.9, 1.6 Hz, 1H), 7.65 (ddd, J = 8.6, 7.2, 1.6 Hz, 1H), 7.53 (dd, J = 8.3, 4.1 Hz, 1H), 7.50–7.46 (m, 2H), 7.39 (dd, J = 8.3, 1.1 Hz, 1H), 7.31 (ddd, J = 8.1, 7.3, 1.1 Hz, 1H), 7.21 (dd, J = 6.0, 3.1 Hz, 1H), 5.91 (s, 1H), 4.28 (t, J = 6.3 Hz, 2H), 4.22 (t, J = 6.4 Hz, 2H), 1.99–1.94 (m, 4H), 1.77–1.71 (m, 2H). ^{13}CNMR (151 MHz, DMSO-d_6) δ 165.48, 162.17, 155.04, 153.26, 149.38, 140.29, 136.22, 133.18, 129.52, 127.31, 124.62, 123.29, 122.26, 119.92, 116.93, 115.77, 109.82, 90.98, 69.92, 68.55, 28.78, 28.18, 22.72. HRMS (ESI): calcd for $C_{23}H_{21}NO_4$ $[M + H]^+$ 376.1549, found $[M + H]^+$376.1557. HPLC: tR = 4.742 min (99.85 %).

4.3. Pharmacological assay

4.3.1. Thioflavin T (ThT) aggregation assay

$A\beta_{1-42}$ was dissolved in DMSO and diluted to 100 μM with 50 mM glycine-NaOH buffer (pH 8.5), test compounds were prepared as 10 mM DMSO stock solutions. A 20 μL mixture which include $A\beta_{1-42}$ (10 μL, final concentration 25 μM) with or without the test compound (10 μL, final concentration 10 μM) was incubated at 37 °C for 48 h, with resveratrol as references. Post-incubation, samples were diluted to 200 μL with 50 mM glycine-NaOH buffer (pH 8.5, 5 μM ThT), and 450 nm fluorescence (excitation: 450 nm, slits: 5 nm) was measured via a Molecular Devices monochromator-based microplate reader (Molecular Devices). Aβ aggregation inhibitory rate was calculated as $(1\text{-}IF_i/IF_c) \times 100$ % (IF_i/IF_c = fluorescence of samples with/without test compound, minus ThT background).

4.3.2. Inhibition studies on ChE

Acetylcholinesterase (*h*AChE, human erythrocyte), butyrylcholinesterase (*h*BuChE, human serum), DTNB, ATC, BTC, and tacrine were from Sigma; donepezil was from Tokyo Chemical Industry. All

analytical-grade reagents were used as received.

All procedures used 0.1 M KH_2PO_4/K_2HPO_4 buffer (pH 8.0). Enzymes were reconstituted in double-distilled water; test compounds were prepared as 10 mM DMSO stocks, then diluted in buffer. The 200 μL assay mixture (buffer, test compound, 0.5 μM DTNB, 0.5 μM ATC/BTC, enzyme) was pre-incubated at 37 °C for 15 min before substrate addition. Absorbance at 412 nm was recorded for 2 min at 37 °C via PowerWave XS2 microplate spectrophotometer, with triplicate assays per concentration. Compounds were first screened for ChE inhibitory activity at 5 μM; those with >50 % ChE inhibitory activity were chosen for determination of their IC_{50} values (Origin 8.0).

4.3.3. Inhibition of BACE1

The inhibitory activity against BACE1 was determined using a commercially available β-Secretase Activity Fluorometric Assay Kit (Sigma-Aldrich, St. Louis, MO, USA; Catalog No. MAK237) according to the manufacturer's instructions, with the provided β-secretase inhibitor serving as the positive control.

4.3.4. Parallel artificial membrane permeation assay[36,37]

The PAMPA assay followed Di et al.'s method: 4 μL of porcine brain phospholipid (PBL, Avanti Polar Lipids) in dodecane (2 % *v*/v) was added onto the membrane of the donor plate, followed by 200 μL of 100 μg/mL solution of the test compound was added. Then the donor plate was placed on acceptor plates which include 300 μL PBS/EtOH (7:3) and incubated 10 h at room temperature. Acceptor solutions were quantified via UV–vis plate reader (Flexstation 3), with ≥3 replicates per sample. Permeability coefficient (P_e) was calculated as: $P_e = -V_d \times V_a/[(V_d + V_a)\ A \times t] \times \ln(1 - drug_{acceptor}/drug_{equilibrium})$ (Vd = donor volume, Va = acceptor volume, A = filter area, t = permeation time). Results are mean ± SD. Fourteen BBB permeability standards (Table S1) validated the method, showing strong linear correlation: P_e (exp.) = 1.1772 P_e (lit.) − 0.8626 ($R^2 = 0.9537$) (Fig. S1). Per Di et al.'s limit (P_e (lit.) = 4.0×10^{-6} cm/s), compounds with $P_e > 3.8 \times 10^{-6}$ cm/s were considered BBB-permeable.

4.3.5. Surface plasmon resonance (SPR)

SPR experiments were performed using a ProteOn® XPR36 system (Bio-Rad) with a GLH sensor chip. $A\beta_{1–42}$ was dissolved to a concentration of 100 μg/mL in filtered/degassed running buffer (20 mM PBS, pH 7.4, 0.005 % Tween-20) and immobilized in flow cells (one as blank control). Test compounds, serially diluted in running buffer, were injected at 25 μL/min for 5 min (association), followed by a 5-min dissociation phase at 25 °C. Sensorgrams were corrected by subtracting blank readings; data were analyzed via ProteOn® Manager Software with Langmuir model fitting. Resveratrol was used as a reference compound for comparison.

4.3.6. Cell viability assay

SH-SY5Y cells were seeded in 96-well plates (1×10^5 cells/well), incubated at 37 °C with 5 % CO_2 for 24 h, then medium was replaced and cells exposed to test compounds (various concentrations) for another 48 h; cell morphology was microscopically recorded. After that, compounds were removed, and cells were treated with 80 μL medium + 20 μL MTT (final concentration 0.5 mg/mL) for 4 h. MTT was discarded, formazan crystals solubilized in DMSO, and absorbance measured at 570 nm via microplate reader. Results are presented as mean ± SD from three independent experiments.

4.3.7. Effect of **B8** on $A\beta_{1–42}$-induced SH-SY5Y cells

$A\beta_{1–42}$ aggregates were prepared per manufacturer's protocol. 100 μM Aβ peptides in DMEM incubated at 37 °C for 48 h. To assess **B8**'s effect on Aβ-induced neurotoxicity, SH-SY5Y cells (2.5×10^3 cells/well) were seeded; after 24 h, cells were pretreated with **B8** (0/2/5/10 μM) for 30 min, then treated with 20 μM Aβ for 24 h. Cell viability was measured via MTT assay.

4.3.8. Analysis of oxidative stress in $A\beta_{1–42}$-induced SH-SY5Y cells

Intracellular ROS was quantified using H_2DCF-DA (oxidized by ROS to fluorescent DCF). SH-SY5Y cells (2×10^5 cells/well, 6-well plates) were seeded, after incubated 24 h, cells were pretreated with test compounds (various concentrations) for 30 min, then exposed to 20 μM $A\beta_{1–42}$ for 10 h. Cells were trypsinized, PBS-washed, resuspended in 500 μL binding buffer, and incubated with 10 μM H_2DCF-DA (serum-free medium, 37 °C, dark, 30 min). Post-incubation, cells were PBS-washed thrice. Fluorescence (excitation 488 nm) was detected via FACSCanto flow cytometer (Beckman Coulter), with ≥10,000 events/replicate (3 independent experiments). Data were analyzed using FlowJo software.

4.3.9. Measurement of cell apoptosis by Annexin V-FITC/PI double staining

SH-SY5Y cells (2×10^5 cells/well) were seeded, incubated 24 h, treated with test compounds for 30 min, then exposed to 20 μM $A\beta_{1–42}$ for 24 h. Cells were trypsinized, PBS-washed, resuspended in 500 μL binding buffer, and mixed with 5 μL Annexin V-FITC +10 μL PI. The mixture was incubated (37 °C, dark, 15 min). PI (610 nm) and Annexin V-FITC (530 nm) fluorescence was measured via flow cytometry (Beckman Coulter); 10,000 cells/sample were analyzed, with results from 3 independent experiments.

4.3.10. The acute toxicology of **B8**

Acute toxicity of **B8** in KM mice (18–22 g, male) was assessed via the Up-and-Down Procedure (UDP, per China FDA guidelines), with a slope factor (σ) of 0.5 (per chemical drug acute toxicity guidelines). Thirty KM mice were randomly divided into 5 groups, given intragastric **B8** (100 μL/10 g body weight) at 0/17.5/55/175/550/1750/2000 mg/kg (starting dose: 17.5 mg/kg). Mice were monitored for abnormal behavior/mortality (continuously first 4 h, intermittently next 24 h, occasionally for 14 days). Mice were finally sacrificed for macroscopic examination of heart/liver/kidney damage. Dose progression stopped when meeting one of AOT425StatPgm (USEPA)'s three stopping rules.

4.3.11. In vivo efficacy of **B8** in AD mice model

Animals: All animal experiments followed the NIH Guide for the Care and Use of Laboratory Animals (NIH Pub. No. 8023, rev. 1978) and were approved by Zunyi Medical University's Animal Experimentation Ethics Committee. Tg mice (C57BL/6, APPsw/PSEN1, 6 months old, male) and age-matched WT mice (C57BL/6, 6 months old, male) were obtained from Huafukang Biotechnology (Beijing, China). Mice were acclimatized for 1 week in a 12 h light/dark cycle (23 °C, 60–70 % humidity) with ad libitum food/water at the laboratory animal center.

Drug treatments: Mice were divided into 4 groups: (1) WT: WT mice given intragastric 0.9 % saline; (2) AD: Tg mice given intragastric 0.9 % saline. (3) Donepezil: Tg mice given intragastric donepezil (2 mg/kg/day); (4) **B8**: Tg mice given intragastric **B8** (10 mg/kg/day, dissolved in 0.9 % saline) for 30 consecutive mornings.

Morris water maze test: On day 24 of drug administration, the Morris Water Maze (MWM) test was conducted on mice (n = 8/group). The apparatus was a 120 cm-diameter, 45-cm-high circular tank (20 ± 1 °C water, 31 cm depth, opaque with non-toxic TiO_2) with a 9 cm-diameter hidden platform (30 cm high, 1 cm below water, first quadrant midpoint). Mice were trained once daily for 5 days (4 rotational starting quadrants, 60s to find the platform; 60s latency if guided). Escape latency was recorded via a computerized video-tracking system (Shanghai Xinruan). A probe test (platform removed) was done 24 h post-training: mice swam freely for 60s. Video-tracking software recorded platform crossings, average speed, target quadrant time/path length, and virtual platform data to assess memory consolidation.

4.3.12. Tissue collection and sample preparation

Four mice from each group were humanely euthanized through overexposure to ether inhalation. Subsequently, their brains were removed, post-fixed in 4 % paraformaldehyde for a duration of 24 h, and subsequently embedded in paraffin. For hematoxylin and eosin (H&E)

staining and immunohistochemistry, coronal sections of 4 μm in thickness were meticulously prepared.

Four mice per group were sacrificed, their brains were quickly removed, hippocampi and cortex dissected on ice, weighed, and homogenized in 0.9 % saline. The homogenate was centrifuged (3000 rpm, 4 °C, 10 min), and the supernatant was used to detect SOD, MDA, and GSH (per kits from Jiancheng Biochemical, Nanjing, China).

4.3.13. HE staining

Paraffin-embedded sections were deparaffinized, rehydrated, stained with hematoxylin (5 min) and eosin (1 min), then dehydrated (graded alcohol), cleared (xylene), and mounted. Hippocampal histopathological changes were examined via computerized image analysis. Degenerated cell index was calculated from 4 representative images/mouse using ImageJ.

4.3.14. Immunohistochemistry

Slides were heat-induced epitope-retrieved in antigen buffer (microwave: 8 min medium heat, 8 min rest, 7 min medium-low heat), cooled to room temperature, then PBS-washed (pH 7.4, 2 × 5 min). Sections were quenched (3 % H_2O_2, 25 min, room temp, dark), PBS-washed twice, blocked with BSA (30 min), then incubated overnight with 1:100-diluted Aβ-14,420, IL-1β, or TNFα antibodies (Abcam). After primary incubation, sections were incubated with 1:500 secondary antibody (50 min, room temp), PBS-washed, treated with DAB, then dehydrated (graded ethanol), cleared (xylene), and cover slipped. The extent of Aβ plaque deposition in the brain was quantified as the percentage of the Aβ-positive area relative to the total area in 4 representative images per mouse using ImageJ software.

4.3.15. Statistical analysis

The data were analyzed using GraphPad Prism 8.0.2 (GraphPad Software Inc., CA). One-way ANOVA followed by Newman−Keuls post hoc test. All data were expressed as mean ± SD, Probability value below 0.05 was considered statistically significant.

CRediT authorship contribution statement

Shun Li: Writing – review & editing, Writing – original draft, Formal analysis, Data curation, Conceptualization. **Xinrui Li:** Formal analysis, Data curation. **Shuanglong Li:** Software, Data curation. **Daoyuan Chen:** Writing – review & editing. **Chunli Xia:** Writing – review & editing, Supervision, Resources, Methodology.

Declaration of competing interest

The authors declare that they have no known competing financial interests or personal relationships that could have appeared to influence the work reported in this paper.

Acknowledgments

This work was financially supported by grants from the National Natural Science Foundation of China (No. 21867020, No. 22007107), the Science and Technology Foundation of Guizhou Province (Qian Ke He J ZK [2022]611, Qian Ke He J ZK [2022]585 and Qian Ke He J ZK [2024]267), Characteristic innovation projects of universities in Guangdong Province (2023KTSCX236), and Zhuhai basic and applied Basic research Foundation (ZH22017003210074PWC)

Appendix A. Supplementary data

Supplementary data to this article can be found online at https://doi.org/10.1016/j.bmc.2025.118499.

Data availability

Data will be made available on request.

References

1. Nativio R, Lan Y, Donahue G, et al. Berger, an integrated multi-omics approach identifies epigenetic alterations associated with Alzheimer's disease. *Nat Genet*. 2020;52:1024–1035.
2. Gonzales MM, Garbarino VR, Pollet E, et al. Biological aging processes underlying cognitive decline and neurodegenerative disease. *J Clin Invest*. 2022;132, e158453.
3. Riessland M, Ximerakis M, Jarjour AA, et al. Therapeutic targeting of senescent cells in the CNS. *Nat Rev Drug Discov*. 2024;23:817–837.
4. Hamuľaková S, Gucký A, Mezencev R, et al. Inhibition of amyloid fibrillization of amyloid β peptide by 4,7-disubstituted coumarin derivatives. *Bioorg Med Chem*. 2025;129, 118302.
5. Nagani A, Shah M, Patel S, et al. Unveiling piperazine-quinoline hybrids as potential multi-target directed anti-Alzheimer's agents: design, synthesis and biological evaluation. *Mol Divers*. 2025;29:1453–1478.
6. Shome A, Jha KT, Chahat Chawla V, Chawla PA. An insight into medicinal chemistry and SAR studies of cholinesterase and BACE-1 inhibitors for Alzheimer's disease. *CNS Neurol Disord Drug Targets*. 2024. https://doi.org/10.2174/0118715273315191241002115155.
7. Francelin C, Mitter SK, Qian Q, et al. BACE1 inhibition increases susceptibility to oxidative stress by promoting mitochondrial damage. *Antioxidants (Basel)*. 2021;10:1539.
8. Fanlo-Ucar H, Picón-Pagès P, Herrera-Fernández V, Ill-Raga G, Muñoz FJ. The dual role of amyloid Beta-peptide in oxidative stress and inflammation: unveiling their connections in Alzheimer's disease Etiopathology. *Antioxidants (Basel)*. 2024;13:1208.
9. Wang R, Reddy PH. Role of glutamate and NMDA receptors in Alzheimer's disease. *J Alzheimer's Dis*. 2017;57:1041–1048.
10. Pathak C, Kabra UD. A comprehensive review of multi-target directed ligands in the treatment of Alzheimer's disease. *Bioorg Chem*. 2024;144, 107152.
11. Yoo J, Lee J, Ahn B, et al. Multi - target-directed therapeutic strategies for Alzheimer's disease: controlling amyloid-β aggregation, metal ion homeostasis, and enzyme inhibition. *Chem Sci*. 2025;16:2105–2135.
12. Sharma P, Sharma S, Yadav Y, et al. Current pharmacophore based approaches for the development of new anti-Alzheimer's agents. *Bioorg Med Chem*. 2024;113, 117926.
13. Avelar M, Delgado-Acosta PF, Guzmán-Ávila RV, et al. Coumarin compounds against Alzheimer's disease: an in-silico approach. *Results Chem*. 2025;16, 102481.
14. Abd El-Mageed MMA, Fattah Ezzat MA, Moussa SA, et al. Rational design, synthesis and computational studies of multi-targeted anti-Alzheimer's agents integrating coumarin scaffold. *Bioorg Chem*. 2025;154, 108024.
15. Rai S, Singh VK, Ahmad I, et al. Design, synthesis, molecular docking, DFT analysis, dynamics simulation and cytotoxicity evaluation of coumarin derivatives as acetylcholinesterase (AChE) inhibitors against alzheimer's disease. *J Mol Struct*. 2025;1329, 141436.
16. Zhong G, Guo J, Pang C, et al. Novel AP2238-clorgiline hybrids as multi-target agents for the treatment of Alzheimer's disease: design, synthesis, and biological evaluation. *Bioorg Chem*. 2023;130, 106224.
17. Jevtić II, Suručić RV, Tovilović-Kovačević G, et al. Multi - target potential of newly designed tacrine-derived cholinesterase inhibitors: synthesis, computational and pharmacological study. *Bioorg Med Chem*. 2024;101, 117649.
18. Li X, Li T, Zhang P, et al. Discovery of novel hybrids containing clioquinol−1-benzyl-1,2,3,6-tetrahydropyridine as multi-target-directed ligands (MTDLs) against Alzheimer's disease. *Eur J Med Chem*. 2022;244, 114841.
19. Umar M, Rehman Y, Ambreen S, et al. Innovative approaches to Alzheimer's therapy: harnessing the power of heterocycles, oxidative stress management, and nanomaterial drug delivery system. *Ageing Res Rev*. 2024;97, 102298.
20. Liu Y, Uras G, Onuwaje I, et al. Novel inhibitors of AChE and aβ aggregation with neuroprotective properties as lead compounds for the treatment of Alzheimer's disease. *Eur J Med Chem*. 2022;235, 114305.
21. Ahmed EY, Serry AM, Aly HF, et al. Design, synthesis and molecular docking studies of tailored coumarin and chromone derivatives for use as anti-Alzheimer agents. *J Mol Struct*. 2025;1323, 140732.
22. Hussain MK, Khatoon S, Khan MF, et al. Coumarins as versatile therapeutic phytomolecules: a systematic review. *Phytomedicine*. 2024;134, 155972.
23. Bala IA, Al Sharif OF, Asiri AM, et al. Quinoline: a versatile bioactive scaffold and its molecular hybridization. *Results Chem*. 2024;7, 101529.
24. Melo L, Silva AMS, Albuquerque HMT. The role of quinoline in the development of near-infrared fluorescent probes for diagnosis of Alzheimer's disease. *Eur J Med Chem*. 2025;296, 117874.
25. Shetab-Boushehri SV. Ellman's method is still an appropriate method for measurement of cholinesterases activities. *EXCLI J*. 2018;17:1611–2156.
26. McKinzie DL, Winneroski LL, Green SJ, et al. Discovery and early clinical development of LY3202626, a low-dose, CNS-penetrant BACE inhibitor. *J Med Chem*. 2021;64:8076–8100.
27. Naik RA, Mir MN, Malik IA, et al. The potential mechanism and the role of antioxidants in mitigating oxidative stress in alzheimer's disease. *Front Biosci (Landmark Ed)*. 2025;30:25551.
28. Chen Y, Lai M, Tao M. Evaluating the efficacy and safety of Alzheimer's disease drugs: a meta-analysis and systematic review. *Medicine*. 2024;103, e37799.

29. Ale T, Ale T, Baker KJ, et al. Delivery of Tempol from polyurethane Nanocapsules to address oxidative stress post-injury. *Bioconjug Chem*. 2025;36:146–151.
30. Mei Z, Zheng P, Tan X, et al. Huperzine a alleviates neuroinflammation, oxidative stress and improves cognitive function after repetitive traumatic brain injury. *Metab Brain Dis*. 2017;32:1861–1869.
31. Weaver DF. Druggable targets for the immunopathy of Alzheimer's disease. *RSC Med Chem*. 2023;14:1645–1661.
32. Knez D, Diez-Iriepa D, Chioua M, et al. 8-Hydroxyquinolylnitrones as multifunctional ligands for the therapy of neurodegenerative diseases. *Acta Pharm Sin B*. 2023;13:2152–2175.
33. Babaei E, Küçükkılınç TT, Jalili-Baleh L, et al. Novel Coumarin-pyridine hybrids as potent multi-target directed ligands aiming at symptoms of Alzheimer's disease. *Front Chem*. 2022;10, 895483.
34. Uliassi E, Bergamini C, Rizzardi N, et al. Quinolinetrione-tacrine hybrids as multi-target-directed ligands against Alzheimer's disease. *Bioorg Med Chem*. 2023;91, 117419.
35. Duarte Y, Fonseca A, Gutiérrez M, et al. Novel coumarin-quinoline hybrids: design of multitarget compounds for Alzheimer's disease. *ChemistrySelect*. 2019;4:551–558.
36. Di L, Kerns EH, Fan K, et al. High throughput artificial membrane permeability assay for blood–brain barrier. *Eur J Med Chem*. 2003;38:223–232.
37. Wohnsland F, Faller B. High-throughput permeability pH profile and high throughput alkane/water log P with artificial membranes. *J Med Chem*. 2001;44:923–930.